

Forecasting corn yield at the farm level in Brazil based on the FAO-66 approach and soil-adjusted vegetation index (SAVI)



Luan Peroni Venancio^{a,*}, Everardo Chartuni Mantovani^a, Cibele Hummel do Amaral^b, Christopher Michael Usher Neale^c, Ivo Zution Gonçalves^c, Roberto Filgueiras^a, Isidro Campos^{d,1}

^a Agricultural Engineering Department, Federal University of Viçosa (UFV), Avenue Peter Henry Rolfs, Viçosa, 36570-900, MG, Brazil

^b Forest Engineering Department, Federal University of Viçosa (UFV), Avenue Peter Henry Rolfs, Viçosa, 36570-900, MG, Brazil

^c Daugherty Water for Food Global Institute, University of Nebraska (UNL), Nebraska Innovation Campus, 2021 Transformation Dr. Ste 3220, Lincoln, NE, 68588, United States

^d Grupo de Teledetección y SIG, Instituto de Desarrollo Regional, Universidad de Castilla-La Mancha (UCLM), Campus Universitario SN, Albacete, Spain

ARTICLE INFO

Keywords:

Corn productivity

Biomass

Remote sensing data

Basal crop coefficient

Vegetation indices

ABSTRACT

Crop yield forecasting at the field level is essential for decision-making and the prediction of agricultural economic returns for farmers. Thus, this study evaluated the performance of a methodology for corn yield prediction in irrigated fields in the western region of the state of Bahia, Brazil. This methodology integrates a time series of the basal crop coefficient (K_{cb}) estimated from the soil-adjusted vegetation index (SAVI) into a simple model based on the water productivity as presented in the FAO-66 manual. In this context, an extensive field-level dataset of 52 center pivot fields of cultivated with corn was used for four consecutive growing seasons (2013 to 2016). Surface reflectance images from the Landsat series were used to calculate the SAVI. The methodology performance was assessed through RMSE, RRMSE, MBE, MAE, and r^2 . The results revealed that the difference between the predicted and actual yield values ranged between -12.2% and 18.8% but that the majority of the estimates remained between -10% and 10%, considering that a single harvest index (HI) was used for the hybrids cultivated in the growing seasons of 2014, 2015 and 2016. After a new reanalysis (by grouping the similar hybrids and using specific HIs), the performance of the predictions increased, especially for the Pioneer hybrids; the majority of the differences between the predicted yield values and the measured yield values remained between -5% and 5%. The results of this research showed that it is essential to work with different HIs when considering different hybrids and years under different weather conditions.

1. Introduction

Yield estimation prior to harvest plays a vital role in agricultural development worldwide (Jin et al., 2018) and is fundamental to world food security, decision-making, and crop management (Mokhtari et al., 2018; Xie et al., 2017). Therefore, it is important to estimate crop yields prior to harvest as aboveground dry biomass (AGB) through an effective methodology such as the use of crop growth models (CGMs). A CGM translates the relationship between plants and the environment and considers the primary biophysical and biochemical processes in the soil-crop-atmosphere system, which include photosynthesis, respiration, transpiration, biomass, yield and senescence, simulating these processes at different time scales (Boote, 1996; Kasampalis et al., 2018; Wang

et al., 2013). However, CGMs have a great limitation for large-scale applications in the lack of spatial information, such as information on different crop varieties, soil types and crop management practices (Guo et al., 2017; Huang et al., 2019; Kasampalis et al., 2018).

Remote sensing (RS) data can provide nondestructive temporal information on plant responses to dynamic weather conditions and management practices at large scales with low cost (Foster et al., 2019; Battude et al., 2016; Frampton et al., 2013; Lin et al., 2009; Veloso et al., 2017). Thus, this technology also shows a large potential for crop yield estimation, as well as variability across fields and years. There are three main approaches of RS methods to estimate biomass and yield, according to Sadras et al. (2018): (a) biomass accumulation models, (b) direct reflectance-based empirical relationships on selected dates and

* Corresponding author.

E-mail addresses: luan.venancio@ufv.br (L.P. Venancio), everardo@ufv.br (E.C. Mantovani), chamaral@ufv.br (C.H. do Amaral), cneale@nebraska.edu (C.M. Usher Neale), ivo.zution@gmail.com (I.Z. Gonçalves), roberto.f.filgueiras@ufv.br (R. Filgueiras), campos.isidro@gmail.com (I. Campos).

¹ Present address: Directorate-General of Agriculture and Rural Development. European Commission. Rue de la Loi 130. Brussels (Belgium).

(c) integration of RS-derived variables into CGM.

The direct reflectance-based empirical relationships on selected dates assume basically that the vigor of the crop canopy, observed in the spectral RS data, is directly related to the yield. These models are relatively simple because these RS data-yield relations are described in simple formulas but without any deeper physiological background (Ferencz et al., 2004; Kasampalis et al., 2018). In addition, these relationships must be locally calibrated, considering the uncertainties related to the selection of the most representative date for the assessment of biomass production and spatial variability (Campos, González-Gómez et al., 2018). Biomass accumulation models normally consider the close relationship between biomass production and the photosynthetically active portion of solar radiation absorbed by the canopy (Daughtry et al., 1992; Liu et al., 2010; Monteith, 1972), while the use of radiation energy for the estimation of plant biomass production represents the fundamental processes that govern crop growth and yield (Liu et al., 2004).

The integration of RS data with a CGM can be achieved by using two distinct methods (Doraismamy et al., 2013). In the first method, a time series of remotely sensed measurements is used to calibrate the CGM. In a second method, the integration is performed by estimating crop parameters (e.g., leaf area index and canopy cover) or vegetation indices from RS data and using them as a direct inputs to the growth model (Maas, 2010). According to Huang et al. (2019), combining CGM and RS data is desirable. In other words, the integration allows us to join the monitoring properties of RS data with the predictive and explanatory abilities of CGM, forming a more effective approach.

Given these advantages, research has been conducted in this direction in recent years for monitoring crop growth status and estimating yield. Examples can be seen in the works of Levitan and Gross (2018) and Ma et al. (2013). It is important to point out that among the several available crop models in scientific literature that can be combined with

RS data, the AquaCrop model is one of those that has been refined and updated to better simulate crop growth status and crop yield (Jin et al., 2018). Thus, the coupling of this model with RS data is very interesting, and a recent example of this combination is a model developed by Campos et al. (2018a,b).

The methodology proposed by these authors integrates a time series of the basal crop coefficient (K_{cb}) into the AquaCrop crop growth and yield partitioning model (Steduto et al., 2012). Then, the K_{cb} is estimated from the soil-adjusted vegetation index (SAVI) (Huete, 1988) by means of a calibrated linear equation (Campos et al., 2017). In sequence, K_{cb} accumulates over a predefined period using numerical integration (Campos et al. (2018a,b)). From K_{cb} accumulated and multiplied by a parameter of water use efficiency for biomass production (WUE^*_B), the potential AGB can be obtained. Therefore, to obtain the actual AGB from the potential, stress by water deficit and thermal stress must be considered in the methodology (Campos et al. (2018a,b)). Finally, the grain yield is estimated by multiplying the actual AGB by a harvest index (HI).

This approach was applied to commercial corn (*Zea mays L.*) fields that were managed in irrigated conditions in the western region of the state of Bahia, Brazil. Corn is considered the third most important crop in this region, occupying an area corresponding to 180,000 ha in 2016/17, with a total production of 1,404,000 tons and an average yield of 7.8 Mg ha⁻¹ (AIBA, 2017). The use of orbital RS data in agriculture, especially in large-scale agriculture (e.g., farms with many central pivots), is essential for decision-making, crop development monitoring, identification of biotic and abiotic stress, and obviously for AGB and yield estimation. However, there is a lack of research on corn yield estimates under real conditions on farms in Brazil. Most of the studies focused on small experimental plots and, when extrapolated to real situations, tended to present a low accuracy.

Considering these aspects, the main objective was to estimate corn

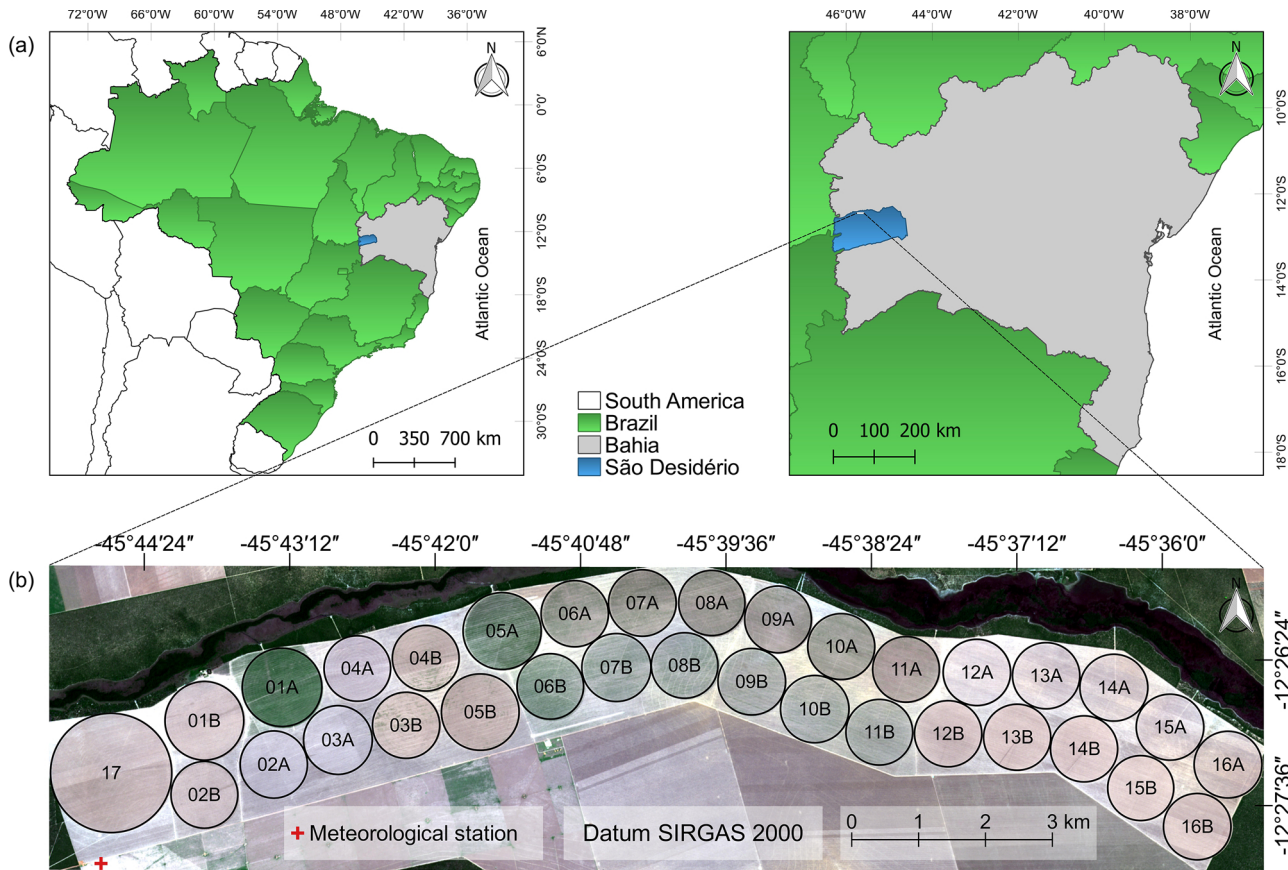


Fig. 1. Location of study area (a), nomenclature and distribution of the center pivots in the fields (b), and meteorological station position.

yield at the farm level in Brazil using a new and simplified RS approach based on the FAO-66 approach and on the SAVI and was initially validated for North American corn production conditions (Campos et al. (2018a,b)). Specific objectives refer to the changes made to the original model, namely: (i) the use of a different methodology for water stress coefficient determination than the FAO-56 approach, (ii) the definition of Kcb accumulation interval based on growing degree days (GDDs) instead of on the SAVI values and (iii) the use of an empirical HI based on previous harvestings and the consideration of the possible effect of the corn variety in the actual values of HI.

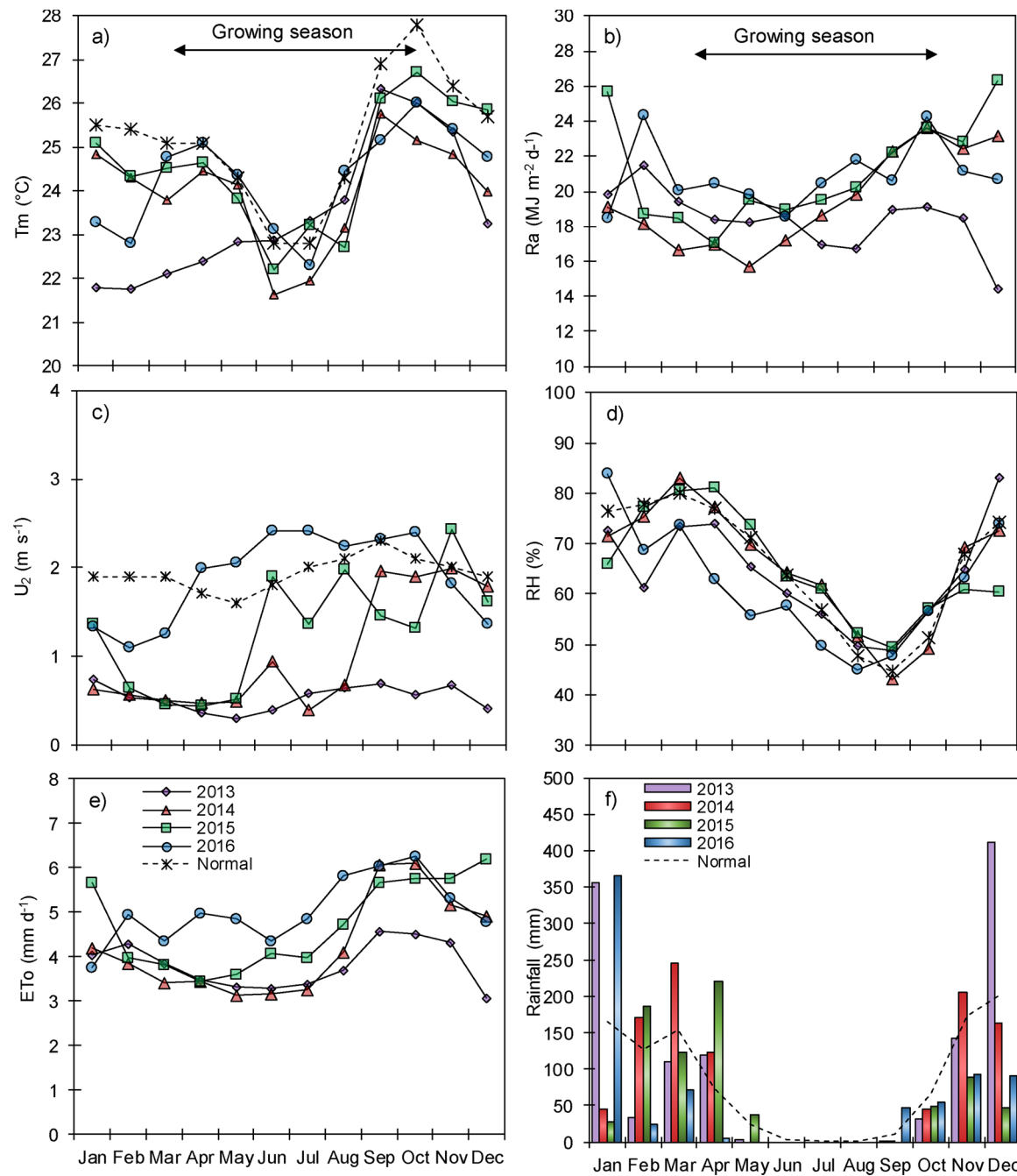
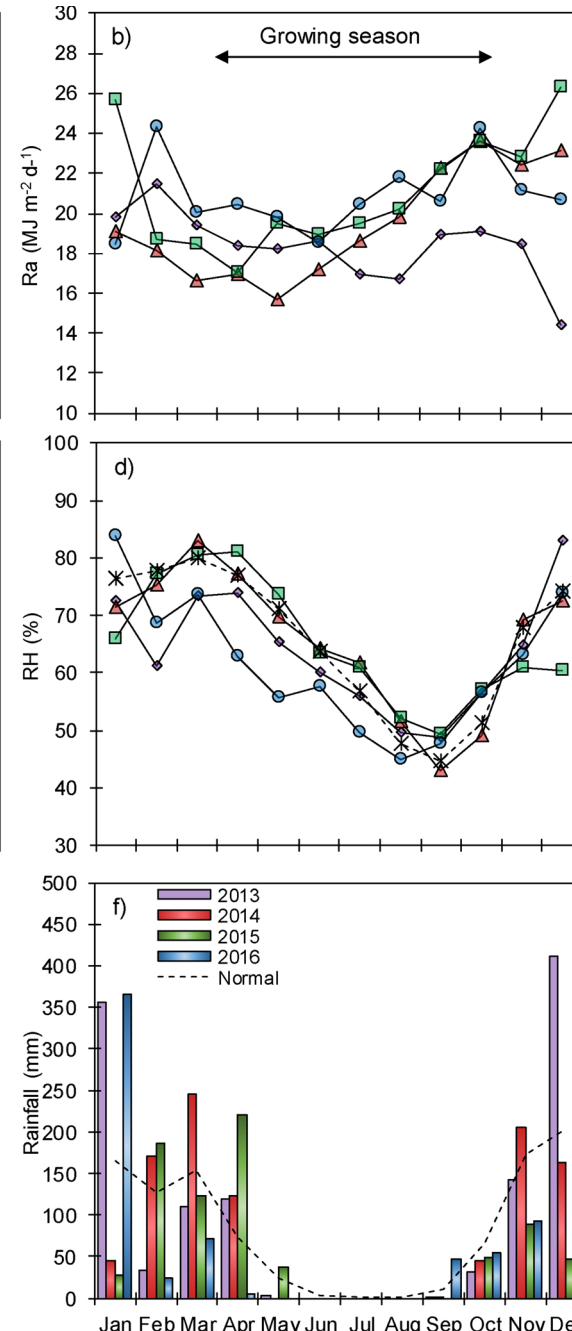


Fig. 2. Comparison of monthly climatic conditions between the growing seasons of 2013, 2014, 2015 and 2016 using averages for mean air temperature (a), extraterrestrial radiation (b), wind speed at 2 m height (c), relative humidity (d), reference evapotranspiration (e) and rainfall (f).

2. Materials and methods

2.1. Study area

The data analyzed in this work were obtained in commercial fields located in the municipality of São Desidério in the western region of the state of Bahia, Brazil (Fig. 1a). The area is located in the rectangle bound by the coordinate pairs: 12°28'08"S-45°45'12"W and 12°25'40"S-45°34'55"W, with an average altitude of 750 m above sea level (Fig. 1b). According to Köppen's climatic classification (Alvares et al.,



2013), the climate of region is a tropical climate (Aw), with a rainy season in summer and a dry winter, with an annual normal precipitation in the region of 1003.4 mm (INMET, 2018), which is concentrated in the rainy season (October to April). Yellow Latosol constitutes the predominant soil type of the fields (Santos et al., 2011). The farm has 17 center pivots, 16 of which are towable, as indicated by the letters A and B in Fig. 1b, and are able to irrigate an area of 1598 ha.

2.2. Field data

The ground and meteorological datasets were obtained during four consecutive corn growing seasons (2013, 2014, 2015 and 2016). Meteorological data such as air temperature (T_m , °C), wind speed at 2 m height (U_2 , $m s^{-1}$), radiation (R_a , $MJ m^{-2} day^{-1}$), relative humidity (RH, %) and rainfall (mm) were obtained from the automated meteorological station located near the fields (Fig. 1b). These data were used to determine the daily reference evapotranspiration (ETo) using the FAO-56 grass reference equation (Allen et al., 1998) and then corn actual evapotranspiration (ET) using the modified FAO method (MFAO) (Mantovani et al., 2006; Mantovani and Costa, 1998). Additionally, temperature data were used to determine the temperature stress coefficient (K_{ST}). The temporal variations in these meteorological data over the four years are shown in Fig. 2. In relation to the ground dataset, the corn hybrids used at each field for each year are presented in Table 1.

2.3. Satellite data - Landsat 8 OLI and Landsat 7 ETM + data

The cloud-free surface reflectance images of the Enhanced Thematic Mapper Plus (ETM+) sensor (Landsat 7) and Operational Land Imager (OLI) sensor (Landsat 8), WRS-2 path 220, row 069 for the corn season (usually April–October) for each year (2013, 2014, 2015 and 2016) were used and downloaded from the archives of the USGS Earth Explorer website (<http://earthexplorer.usgs.gov/>). We acquired 57 images of the study area, including images from both OLI and ETM+ sensors, for the crop seasons of 2013, 2014, 2015 and 2016. The number of images used for yield estimation varied by pivot and season, according to different sowing dates and the presence of clouds in the area of interest. However, two criteria were adopted: (i) at least four images were used per center pivot, and (ii) among the four images, there had to be an image with a date close to the beginning, middle and end of the crop cycle to adequately describe it. The dates with available images are shown in Fig. 3.

Table 1
Corn hybrid yields used by field and year.

2013			2014			2015			2016		
Field	Hybrid	Yield, $Mg ha^{-1}$									
01A	H5	9.87	01B	H9	10.68	01A	H1	10.55	03B	H2	12.61
02A	H4	5.38	02B	H9	11.74	04A	H7	11.05	04B	H9	12.70
03A	H4	4.98	03B	H9	11.24	05A	H9	12.18	05B	H9	13.30
04A	H5	9.89	04B	H9	11.12	06B	H9	11.16	06A	H6	11.65
05A	H4	5.33	05B	H3	11.55	07B	H9	12.14	07A	H6	11.80
06B	H4	6.04	06A	H3	10.06	08B	H9	12.42	08A	H7	11.58
07B	H4	6.94	07A	H3	10.72	09B	H9	12.99	09A	H3	12.38
08B	H4	6.84	08A	H3	10.09	10B	H9	12.49	10A	H3	12.10
09B	H4	7.64	09A	H7	11.21	11B	H9	12.79	11A	H10	12.94
10B	H4	6.95	10A	H7	11.50	12A	H9	11.85	12B	H9	12.05
11B	H4	6.34	11A	H7	10.88	13A	H9	13.02	13B	H9	12.80
12B	H4	7.16	12A	H6	10.83	14A	H9	12.41	14B	H9	12.45
–	–	–	–	–	–	15A	H9	12.49	15B	H9	13.50
–	–	–	–	–	–	16A	H9	12.26	16B	H9	13.00

Hybrids names: Dekalb DKB 390 Pro (H1), Dow AgroSciences 2B810 (H2), Pioneer 30F35 (H3), Pioneer 30F53 (H4), Pioneer 3431 (H5), Pioneer P2830 (H6), Pioneer P3646 (H7), Maximus Viptera 3 (H8), Status Viptera 3 (H9) and Supremo Viptera (H10).

2.4. Basis of the model for the estimation of the aboveground dry biomass (AGB) and grain yield

According to the methodology of Campos et al. (2018a,b), aboveground dry biomass (AGB, in $g m^{-2}$) is estimated as the product of a normalized water use efficiency for biomass production (WUE^*_B , in $g m^{-2}$) times the adjusted basal crop coefficient ($K_{cb,adj}$, dimensionless). $K_{cb,adj}$ is estimated through the product of the basal crop coefficient (K_{cb}), of the water stress coefficient (K_{SW}) and a temperature (cold) stress coefficient (K_{ST}). The relationship between the factors affecting biomass production is presented in Eq. (1).

$$AGB = WUE^*_B \times (\sum K_{cb} \times K_{ST} \times K_{SW}) \quad (1)$$

Yield (grain) is estimated as the product of the simulated AGB multiplied by the HI (Eq. (2)). The HI represents the ratio of weight (grains/plant) to the aboveground dry biomass (Caviglia et al., 2014).

$$Yield = AGB \times HI \quad (2)$$

In this work, the same principles were applied; however, some changes were necessary to make the original model applied to Brazilian farm conditions. Thus, all the terms of Eqs. (1) and (2) are discussed below, with the focus on performed changes. Fig. 4 provides the overall processes followed in this study.

2.4.1. Normalized water use efficiency for biomass production (WUE^*_B)

Campos et al. (2018a,b) used the normalized water use efficiency for biomass production (WUE^*_B), which is commonly referred to as the normalized crop water productivity (WP*) (Raes et al., 2009, 2017; Razzaghi et al., 2017; Steduto et al., 2007; Vanuytrecht et al., 2014). The WP* is considered constant for a given climate and crop, and it is set between 30 and 35 $g m^{-2}$ for C4 crops (Raes et al., 2017). The WUE^*_B in this study was considered to be $33.4 g m^{-2}$ for irrigated corn, a value calibrated by Campos et al. (2018a,b) and in accordance with the one recommended in the FAO-66 approach (i.e., $33.7 g m^{-2}$) (Steduto et al., 2012).

2.4.2. Basal crop coefficient (K_{cb})

The K_{cb} is estimated based on the soil-adjusted vegetation index (SAVI) (Huete, 1988) through Eq. (3), which was developed by Campos et al. (2017) and considers short grass for reference evapotranspiration.

$$K_{cb} = 2 \times SAVI - 0.17 \quad (3)$$

The adjusted K_{cb} is daily by the water and temperature stress and accumulated during a specific period of the growing season. Campos et al. (2018a,b) defined the interval for K_{cb} accumulation based on the

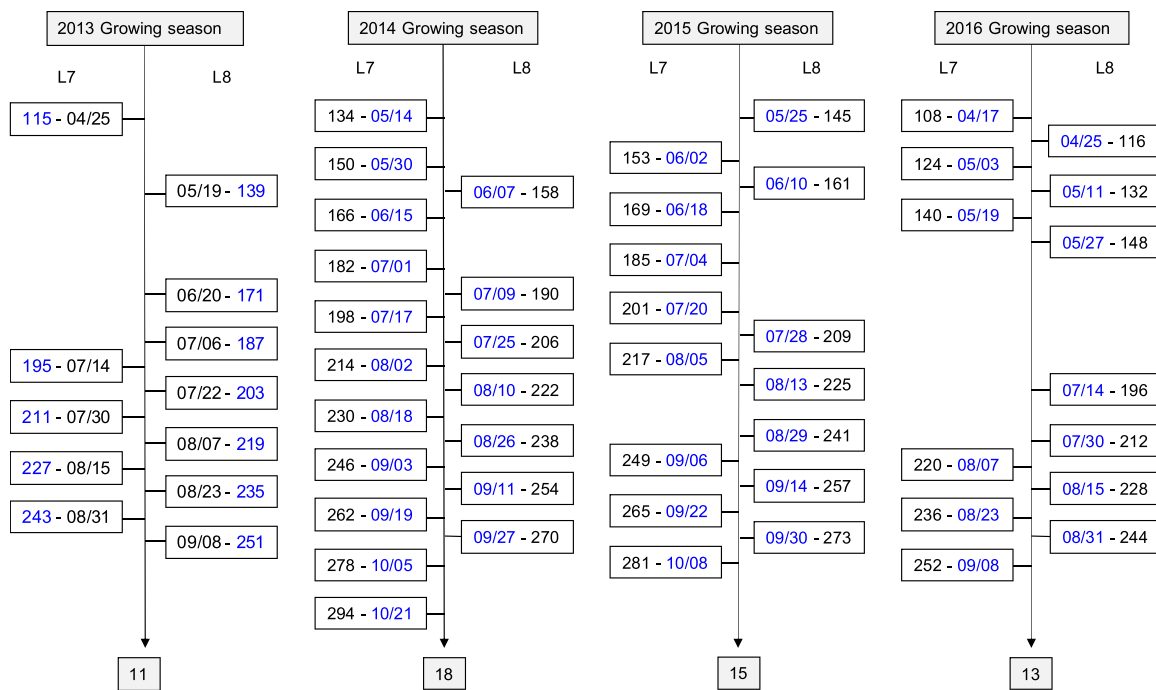


Fig. 3. Day of year (DOY) (in black) with respective date (in blue) of Landsat 7 (L7) and Landsat 8 (L8) images, with the respective number of total images (For interpretation of the references to colour in this figure legend, the reader is referred to the web version of this article).

SAVI values. These values are 0.20 and 0.40 for the start and end, respectively. Pretests based on the abovementioned SAVI values for biomass accumulation show very high estimates for Brazilian conditions (AGB above 35 Mg ha⁻¹). We investigated the possible causes of these overestimates based on the corn crop development and on the photoassimilate distribution in the plant throughout the cycle. It has been verified in many studies that during the grain filling period there is a considerable remobilization of the dry matter that has accumulated in the vegetative parts of corn plants (*i.e.*, the stalk, leaf sheaths and leaves), mainly that in the stalk, to the grains, which assists with their filling, along with the continuation of the photosynthetic process to meet the needs of the reproductive phase (Allison and Watson, 1966; Rajcan and Tollenaar, 1999; Sangoi et al., 2002, 2001).

Based on this, to avoid an overestimate (due to the translocation of photoassimilates during the reproductive period), a new period based on growing degree days (GDDs) was used to obtain daily Kcb through interpolation from the V₂ corn stage, when the plant has two fully emerged leaves and then is able to start the photosynthetic process (Fancelli and Dourado Neto, 2000), until the end of the R₅ stage, which is called “Dent”. It is important to point out that in this stage, the grains would have already accumulated most of their maximum dry weight that would be reached at physiological maturity (Hanway, 1966). The GDD values corresponding to the initial and final periods of Kcb accumulation were 250 and 1500, respectively, based on the study of Martins et al. (2017). In terms of DAS, this is from ± 14 DAS until ± 110 DAS, a similar interval to the one adopted by Kross et al. (2015) for corn biomass estimation.

2.4.3. Water stress coefficient (K_{SW})

The water stress coefficient shows how crop transpiration is affected by water stress or irrigation water deficits. The model of Campos et al. (2018a,b) uses the approach proposed in the FAO-56 manual (Allen et al., 1998). In Brazil, however, especially in irrigated commercial farms that have adopted any type of irrigation management, it is very hard to use the FAO dual-Kc approach and consequently the K_{SW} because of its greater complexity for application. In Brazil, it is more common to use a simpler methodology, such as that proposed by

Bernardo (1989), according to Eq. (4). This methodology was used to obtain the water stress coefficient (K_S) in areas of this study instead of the FAO K_{SW} . The methodology can be described as follows:

$$K_S = \frac{\ln(1 + CSWS)}{\ln(1+SWS)} \quad (4)$$

where SWS is the total soil water storage (mm) and CSWS is the current soil water storage (mm) at a certain time.

2.4.4. Temperature stress coefficient (K_{ST})

The temperature stress coefficient (K_{ST}) was used according to Raes et al. (2009). These authors proposed a logistic relationship between K_{ST} and the relative water stress level (S_{relT}). Numerically, S_{relT} is a linear function of the daily mean air temperature (T_m), and the extremes for the canopy development are T_b and T_o (Eq. (5)).

$$S_{relT} = \frac{T_o - T_m}{T_o - T_b} \quad (5)$$

If mean temperature (T_m) > optimum temperature (T_o), K_{ST} is equal to 1, and if T_{mean} ≤ T_o, K_{ST} is obtained using Eq. (6) (Raes et al., 2009), as follows:

$$K_{ST} = \frac{(S_n \times S_x)}{S_n + (S_x - S_n)^{exp(-r(1-S_{relT}))}} \quad (6)$$

where T_b and T_o for corn are 10 °C and 30 °C, respectively (Steduto et al., 2012), S_x and S_n are the upper and lower limits of K_{ST} and are assumed to be equal to 1.0 and 0.001, respectively, and r is the rate factor (15).

2.4.5. Harvest index (HI)

Campos et al. (2018a,b) suggested a new approach to determine HI based on the hypothesis that the final yield is better correlated with the maximum biomass reached by the crop, in contrast to the relationship between yield and biomass at harvesting. However, the disadvantage of this methodology is the necessity of using grain yield to determine HI. In addition, these authors highlighted that the methodology needs to be validated with additional experiments and analyses.

On the other hand, there are several studies about HI determination

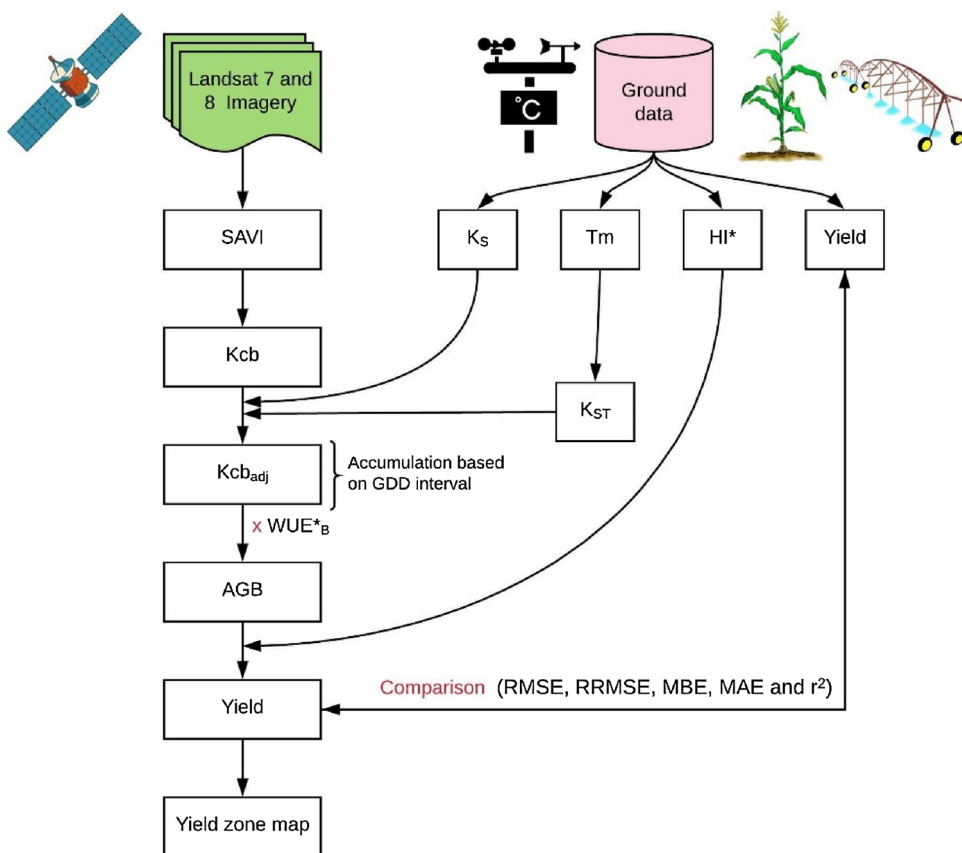


Fig. 4. Step-by-step flowchart following the estimation and evaluation of corn yield at the farm level in Brazil. HI* indicates that it was determined in both the literature and field estimates reported by the agronomist of the farm. K_s, similar to K_{sw}, refers to the water stress coefficient.

for corn, and most of them show values varying between 0.35 and 0.6. Examples can be seen in the works of Bastiaanssen and Ali (2003); O'Shaughnessy et al. (2017); Wang et al. (2018) and Zhai et al. (2017). However, the most common values remain between 0.4 and 0.5 (Bocianowski et al., 2019; Demétrio et al., 2008; Hütsch and Schubert, 2018, 2017; Djaman et al., 2013; Li et al., 2015). Thus, due to the above-cited limitation, the value of 0.45 was chosen for HI.

In the growing season of 2013, a severe and sporadic attack of the bacterium *Erwinia chrysanthemi* pv. Zeae, which causes a disease called "stalk rot of maize", directly affected the HI values. The center pivots 02A, 03A, 05A, 06B, 07B, 08B, 09B, 10B, 11B and 12B were the most affected, while 01A and 04A were slightly less affected. Thus, for the less affected center pivots, the HI was 0.37, and for the most affected, the HI was 0.24. The HI values for 2013 were calculated using Eq. (7) as follows:

$$HI_{2013} = \frac{Y \times 0.45}{X} \quad (7)$$

where HI₂₀₁₃ refers to HI for the year 2013; Y is the average yield for center pivots in 2013 (02A, 03A, 05A, 06B, 07B, 08B, 09B, 10B, 11B and 12B or 01A and 04A); 0.45 is the HI value used for 2014, 2015 and 2016; and X is the average yield for the years of 2014, 2015 and 2016.

2.5. Data analysis

To assess the accuracy of the estimations, the statistical indicators root mean square error (RMSE), relative RMSE (RRMSE), mean bias error (MBE), mean absolute error (MAE) and coefficient of determination (r^2) between the estimated and measured values were calculated. The Tool for Numerical Integration pixel by pixel (TONI_{ppb}) was applied for data processing and analysis. The TONI_{ppb} was developed by the GIS and Remote Sensing Group from the Instituto de Desarrollo

Regional (University of Castilla-La Mancha, Spain) in the frame of the project FATIMA (<http://fatima-h2020.eu>). In the present study, TONI_{ppb} was used to obtain the accumulated value of the relation K_{cb}: K_{ST}. K_s within a date interval defined based on GDDs.

3. Results and discussion

3.1. Irrigation management data

The total irrigation applied in each center pivot varied little from year to year and from pivot to pivot due to the small variation in climatic conditions and its effect on ET₀ (Table 2). The year 2013 had the smallest irrigation depth applied (~400 mm) because of a sporadic and severe stalk rot disease in the corn fields during this season, which influenced irrigation management and strongly impacting the corn yield. The growing cycle of 2016 had the highest mean value of ET, with 648.7 mm (Table 2). This is a result of the high values of temperature and solar radiation but mainly of the wind speed and low relative humidity observed during that year (Fig. 2).

3.2. Water stress coefficient (K_s) and temperature stress coefficient (K_{ST})

Fig. 5 shows the daily K_s values for four selected center pivots, as determined by the model of Bernardo (1989) for the irrigation seasons of 2013–2016. Generally, during all the growing seasons, the K_s values were close to 1, except at the beginning of the growing season after sowing and in the late season, when irrigation intervals are longer because corn has almost reached physiological maturity (Fig. 5).

Bernardo's methodology causes a logarithmic decrease in the K_s value with the reduction in total soil water storage (see Eq. (4)) unlike the FAO-56 approach, which considers a fraction of the total soil water

Table 2

Accumulated values of irrigation (Irr), actual corn evapotranspiration (ET), and reference evapotranspiration (ET₀) during the growing season for each field analyzed in the corn growing seasons of 2013, 2014, 2015 and 2016.

Field-	Irr mm	ET mm	ET ₀ mm	Field -	Irr mm	ET mm	ET ₀ mm
2013				2014			
01A	519.3	300.9	333.1	01B	820.2	569.6	580.6
02A	383.2	283.8	310.9	02B	747.5	547.6	574.6
03A	393.6	290.9	320.5	03B	747.2	544.8	571.6
04A	485.6	296.7	329.9	04B	790.8	555.4	580.8
05A	426.7	301.6	324.6	05B	807.4	556.9	578.9
06B	369.9	244.9	271.3	06A	821.6	599.3	624.4
07B	357.7	246.7	274.0	07A	826.7	594.8	622.7
08B	353.9	251.0	276.9	08A	832.6	595.1	620.1
09B	343.0	252.6	280.2	09A	796.5	594.8	614.0
10B	368.7	264.8	293.9	10A	810.8	591.9	610.8
11B	422.6	271.9	286.5	11A	784.6	580.0	598.2
12B	392.3	273.3	305.2	12A	760.3	504.8	589.3
2015				2016			
01A	745.0	571.2	611.3	03B	703.6	610.7	737.5
04A	737.9	594.8	619.7	04B	780.1	703.4	786.6
05A	587.4	519.2	535.2	05B	847.4	706.7	766.6
06B	768.8	634.9	685.6	06A	688.2	609.7	729.8
07B	766.0	631.0	684.2	07A	707.4	656.8	758.8
08B	771.4	629.3	682.2	08A	733.9	713.0	798.9
09B	747.2	626.2	679.1	09A	756.7	719.8	804.4
10B	772.4	623.5	676.1	10A	766.0	683.6	755.9
11B	772.5	622.8	673.5	11A	676.3	546.0	654.5
12A	710.4	570.5	606.8	12B	686.0	598.4	654.7
13A	708.6	565.6	595.6	13B	698.0	592.7	646.5
14A	750.7	563.7	592.5	14B	754.7	645.5	739.7
15A	698.7	561.1	586.8	15B	714.2	637.1	740.5
16A	737.0	557.4	581.0	16B	756.8	658.9	747.2

available in the root zone that the crop can extract without suffering water stress. Then, Bernardo's K_s is more limiting to the estimation of crop transpiration than is the FAO-56 method. In this sense, it is possible to affirm that cultivated fields did not have any problems with water stress, as K_s remained close to 1, and high yields were obtained in the fields (Table 1), which did not occur in the presence of a water deficit.

During the growing season of 2013, the period of irrigation had a duration of ~ 100 days (Fig. 5a) due to the phytosanitary problem. In the other years (Fig. 5b-d), the period extended to approximately 125 days when the corn reached physiological maturity and the irrigation ended. However, regardless of the irrigation management duration, the K_s values were very similar among the four seasons analyzed.

Fig. 6 shows the temperature (cold) stress coefficient (K_{ST}) for the corn growing seasons of 2013, 2014, 2015 and 2016. The lowest values of K_{ST} were observed during the initial days of the winter in Brazil, which starts in late June, with the lowest value occurring in 2015. The average values of K_{ST} were 0.96 for 2013 and 2014 and 0.97 for 2015 and 2016, indicating that cold stress has a low impact on biomass production under the Brazilian conditions. These results are expected because of the tropical climate, and although corn is cultivated during the autumn/winter season, the air temperatures of the region during this period are compatible with those required for corn (25 and 30 °C) (Fancelli and Dourado Neto, 2000).

3.3. Corn crop development based on SAVI

Understanding patterns of vegetation based on VI is essential for crop management and helps farmers in decision-making. Fig. 7 shows the patterns of temporal evolution of the SAVI in each center pivot over the growing seasons of 2013, 2014, 2015 and 2016. In the four seasons analyzed, it is possible to observe very similar behavior, with a fast increase at the start of the growing cycle, a stability during the mid-

season and a reduction at the end. The lowest SAVI values are observed in the first and sixth images (e.g., June 07 and Oct 21, Fig. 7b) because of the larger amount of exposed soil and plant senescence, respectively, in these periods.

On the other hand, from the second to the fourth image, the highest values of the SAVI were verified, which are mainly a consequence of leaf area increase (Campos et al., 2017; Gitelson et al., 2003). The highest SAVI values in corn plants are normally observed from 60 DAS, when plants tend to reach the maximum leaf area (Kross et al., 2015; Lizaso et al., 2005; Lukeba et al., 2013; Soleymani, 2018; Soufizadeh et al., 2018) until 80 DAS, when the plants are in the silking stage (Hanway, 1966).

Fig. 8 shows the curves of the SAVI values from the four selected center pivots in each growing season along with the positions of the stages (V_2 and R_5) and the respective accumulated GDD values (250 and 1500), which define the beginning and end periods of the Kcb accumulation (Fig. 8c). During all seasons, the evolution of the SAVI according to the four major crop development stages can be clearly observed, with fast increases during the early season and the opposite at the end (fast decrease). During the mid-season, few changes occurred in the crop canopy; thus, the SAVI stayed practically stable. These results corroborate the importance of using satellites with high temporal resolution, as done in the present study with Landsat 7 and 8, to study crops with fast development, such as corn, soybean and bean, to monitor the main changes in the crop.

The SAVI values during the four seasons ranged from 0.12 to 0.72, with an average value of approximately 0.5. Although the maximum value reached 0.72 a few times, most of the maximum values were between 0.68 and 0.7 (Fig. 8), which are the most common in corn fields (Bausch, 1993; Campos et al., 2017). The minimum values varied between 0.12 and 0.20, with great similarity among the four seasons (Fig. 8). Generally, vegetation conditions were slightly variable between fields over the four growing seasons, with very close amplitudes and average SAVI values (Fig. 8). This was a consequence of the high technological level adopted on the farm, which mainly involved high-performance hybrids and correct irrigation management.

3.4. Adjusted basal crop coefficient ($K_{cb,adj}$)

The basal crop coefficient is defined as the ratio of crop evapotranspiration over the reference evapotranspiration when the soil surface is dry, but transpiration is occurring at a potential rate (i.e., water is not limiting transpiration). However, when water is limited in the soil, there is a reduction in Kcb values, which can be calculated by multiplying them by a water stress coefficient (Allen et al., 1998). Campos et al. (2018a,b) demonstrated the clear relationship between AGB production and the accumulated values of Kcb derived from satellite data and, subsequently, the compatibility of the Kcb data derived from satellite images with the transpiration coefficient described in the FAO-66 manual (Allen et al., 1998).

In addition, they also considered temperature (cold) stress on Kcb instead of only water stress (Allen et al., 1998); in other words, the Kcb was adjusted of water deficit and cold temperature stress (Campos et al. (2018a,b)). Fig. 9 shows the map of the Kcb that was adjusted for temperature and water stress conditions ($K_{cb,adj}$) of each irrigated corn field in the four consecutive growing seasons (2013 to 2016). The $K_{cb,adj}$ ranged from 69 to 94, with average values of 79.3, 75.2, 81.6 and 87.9 for 2013, 2014, 2015 and 2016, respectively (Fig. 9). The results obtained in this study were similar to those of Campos et al. (2018a,b), which were obtained under the conditions of Nebraska (USA).

Although the 2013 growing season had problems with a disease (stalk rot of maize), the $K_{cb,adj}$ was slightly higher than that in 2014 (Fig. 9a), as the symptoms of attack became more evident after the period of Kcb accumulation (the end of the R_5 stage), since the attack occurred close to physiological maturation of the grains (the R_6 stage). The 2016 growing season had the highest values among the four

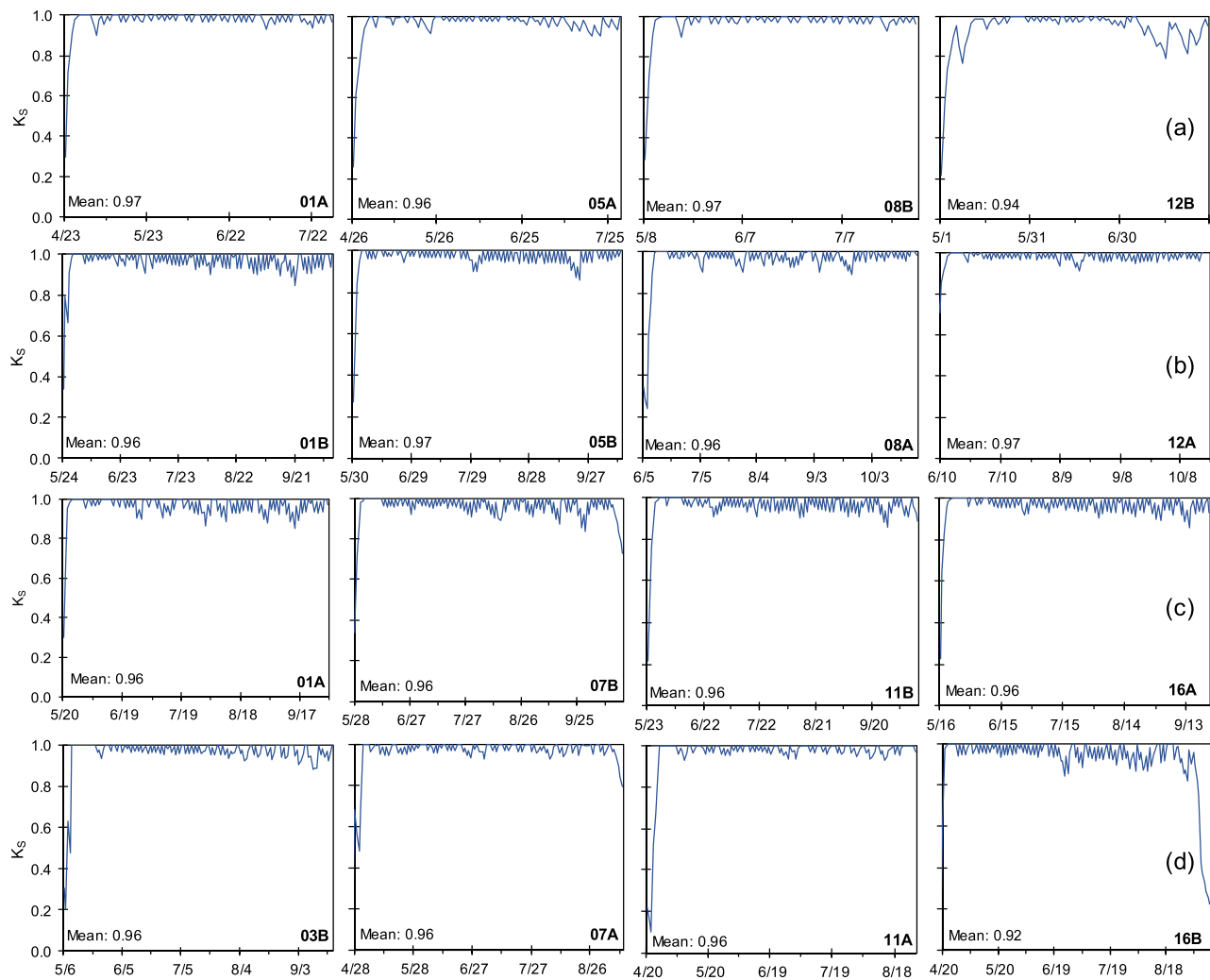


Fig. 5. Temporal evolution of the water stress coefficient (K_s) obtained in selected center pivots in 2013 (a), 2014 (b), 2015 (c) and 2016 (d).

growing seasons (Fig. 9b), which is directly related to the relatively high yield. Generally, the $K_{cb,adj}$ values showed little variation within the same season, and most of this small difference can be attributed to the cultivation of different corn hybrids (Table 1).

3.5. Aboveground dry biomass (AGB) and grain yield

The $K_{cb,adj}$ times WUE^*_B determine the actual AGB. The data referring to AGB are presented in Fig. 10, which shows that AGB ranged between 18

and 34 Mg ha^{-1} . These results can be compared to the findings of Campos et al. (2018a,b), Kross et al. (2015) and Yang et al. (2017). Relatively low AGB was observed in 2013 and 2014 (Fig. 10a) in comparison to 2015 and 2016 (Fig. 10b), with the highest AGB occurring in 2016 (Fig. 10b). In general, the fields had an evolution of production over the season, which can be seen better in the yield results presented in the sequence. It is important to point out that AGB can undergo considerable variations as a function of the WUE^*_B adopted because this value, even if normalized, is variable between 30 and 35 g m^{-2} (Raes et al., 2017).

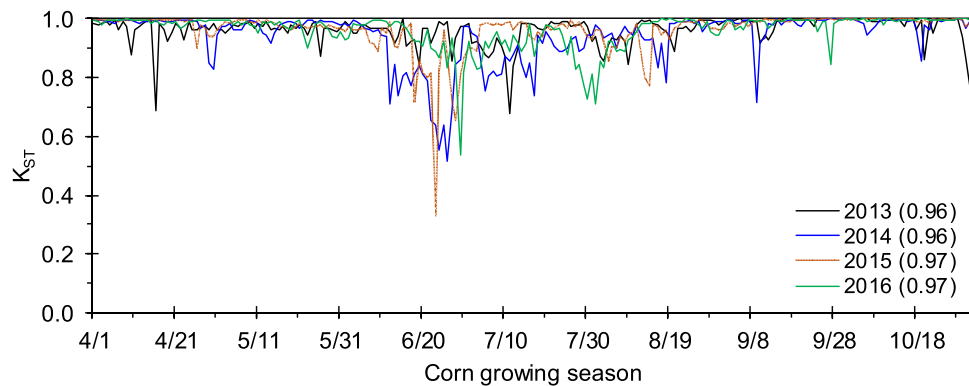


Fig. 6. Temporal evolution of the temperature stress coefficient (K_{ST}) and average values (between parentheses) during the corn growing seasons of 2013, 2014, 2015, and 2016.

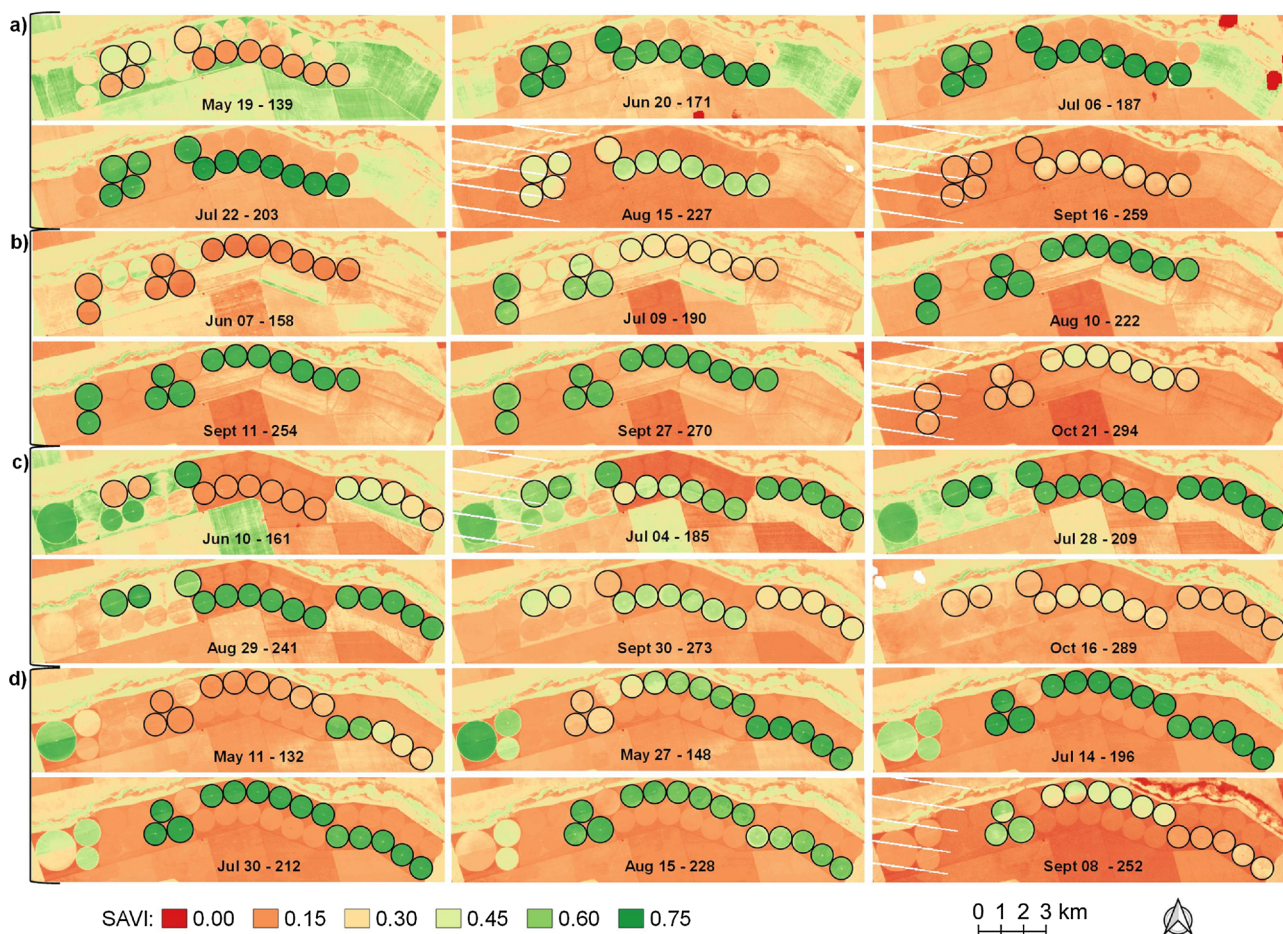


Fig. 7. Maps of the temporal evolution of the SAVI derived from selected Landsat 7 and 8 images for the center pivots cultivated (dark edge) in the growing seasons of 2013 (a), 2014 (b), 2015 (c) and 2016 (d).

Fig. 11 shows the measured versus estimated of corn grain yields for the growing seasons of 2013, 2014, 2015 and 2016. In 2013, the lowest yield among the four seasons was verified, with some values near 5 Mg ha^{-1} (**Fig. 11a**), which is considered very low given the level of technology adopted at the farm. These results are a consequence of an attack of the bacterium *Erwinia chrysanthemi* pv. *zeae*. Regarding the estimation performance of 2013, good agreement was observed with $r^2 = 0.87$. Based on RRMSE (8.3%), which is expressed as a percentage, where lower values indicate less residual variance, good agreement is also observed (**Fig. 11a**). The statistical parameters were also good, with the RMSE equal to 0.573 Mg ha^{-1} and the MAE equal to 0.489 Mg ha^{-1} , with slight underestimation ($\text{MBE} = -0.032 \text{ Mg ha}^{-1}$).

In the 2014 harvest, the regression was not statistically significant, which means that there was no relationship between the measured and estimated data (**Fig. 11b**). Additionally, compared to that in 2013, there was a large decrease in r^2 in 2014 (**Fig. 11a**). On the other hand, RMSE and MAE showed small differences in 2014. The RRMSE was 5.1%, while the MBE indicated overestimation (0.330 Mg ha^{-1}). Regarding the 2015 growing season, the RMSE (NRMSE) between the measured and simulated values was 0.646 Mg ha^{-1} (5.3%), and the r^2 had good improvement (0.45) compared to the previous year (**Fig. 11c**). The MBE was 0.141 Mg ha^{-1} , which was a relatively low overestimate considering the average yield, while MAE was 0.534 Mg ha^{-1} .

As well as in 2014, the regression value for the 2016 growing season was not statistically significant, presenting the worst results of the four seasons analyzed, with $r^2 = 0.03$ and RMSE greater than 1 (1.030 Mg ha^{-1}) (**Fig. 11d**). The RRMSE was similar to that in 2013 (8.3%). The MBE and MAE confirmed that the values estimated for 2016 were poor, with an overestimate reaching 0.727 Mg ha^{-1} and

MAE equal to 0.911 Mg ha^{-1} . In the 2016 growing season, six different corn hybrids were sown, making it the season with the highest number of hybrids, which may have contributed to these poor results due to the use of a single HI ($\text{HI} = 0.45$) for six hybrids.

Fig. 12 shows the absolute difference in percentage between estimated and measured values of yield for the growing seasons of 2013, 2014, 2015 and 2016. The highest difference was observed in 2013 (pivot 03A), with a value of 18.8%, followed by 17.9% in field 02A in 2013 (**Fig. 12a**). The 2014 growing season had only one value greater than 10% (**Fig. 12b**), as did the 2015 growing season (**Fig. 12c**), while 2016 had the greatest amount of error values higher than 10% (**Fig. 12d**). Additionally, in some cases, the differences were less than 1%, and the majority remained between -10 and 10%.

Overall, there were no good results of estimated yield in **Fig. 11**, although the differences presented in **Fig. 12** can be considered low, probably as a consequence of the use of a single HI value for different hybrids and, consequently, their joint analysis. For this reason, considering the two groups, a new analysis was performed on (**Fig. 13**): (i) the Pioneer hybrids and (ii) the Status Viptera 3 hybrid, using data from the growing seasons of 2014, 2015 and 2016 (2013 was excluded because of disease occurrence). Regarding the Pioneer hybrids, which had three different hybrids planted during the abovementioned harvests (i.e., Pioneer 30F35, Pioneer P2830 and Pioneer P3646), the grouping was based on their similarities (Pioneer, 2017) and according to field supervisor, who directly observed the corn hybrid phenology within fields.

These two groups of hybrids represented 92.5% of the cultivated area at the farm during the four seasons, as shown in **Table 1**. Thus, an HI of 0.43 was used for Pioneer hybrids because of their low relatively

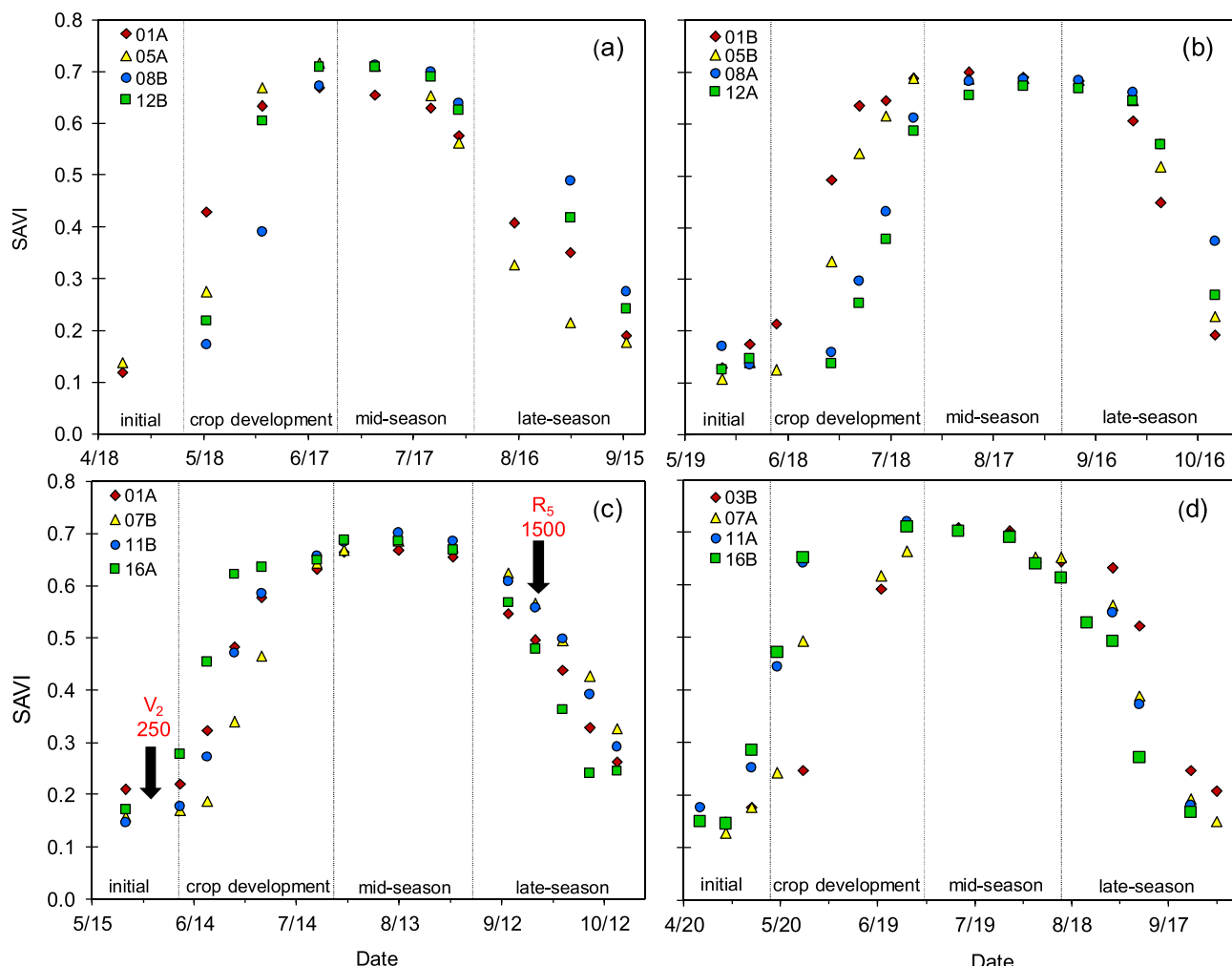


Fig. 8. Temporal evolution of the SAVI for selected fields in the corn seasons of 2013 (a), 2014 (b), 2015 (c) and 2016 (d) along with the position of stages (V_2 and R_5) and the respective accumulated GDDs (250 and 1500), which mark the start and end of the periods of K_{cb} accumulation, respectively, throughout season (c).

yield, while a value of 0.45 was maintained for Status Viptera 3. It is also important to mention the possible effect of planting density (PD) on final yield since the different PD values were used in the fields. However, this aspect was not considered here because the differences

were small (means of 70,286 and 72,000 for Pioneer and Status Viptera 3 hybrid, respectively).

A significant correlation between the observed and predicted yields was observed when considering the hybrids separately (Fig. 13). In

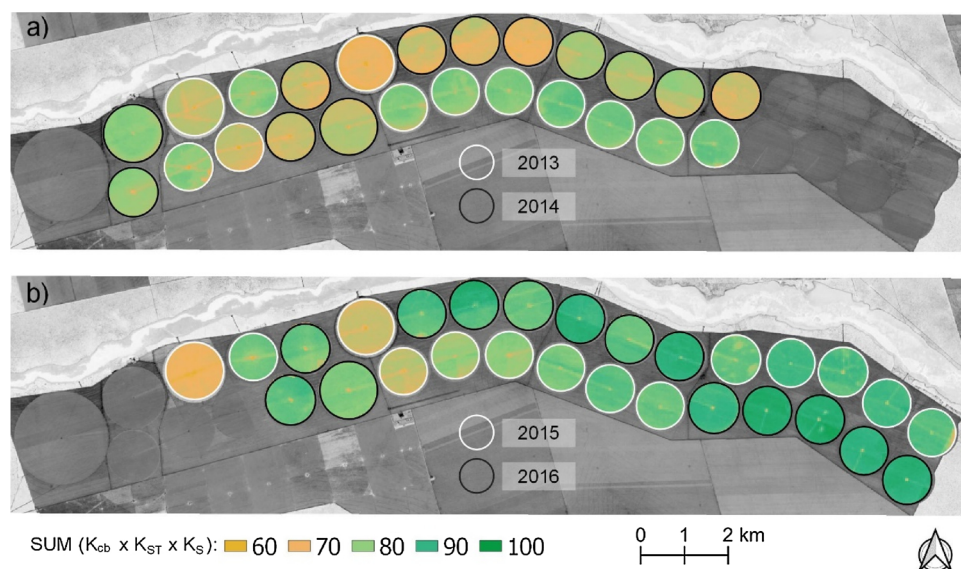


Fig. 9. Map of the accumulated adjusted basal crop coefficient for temperature and water stress conditions ($\Sigma K_{cb} \cdot K_{ST} \cdot K_S$) of each irrigated corn field in the four consecutive growing seasons (2013–2016). The white circles correspond to the center pivots of 2013 and 2015 and the black circles correspond to center pivots of 2014 and 2016.

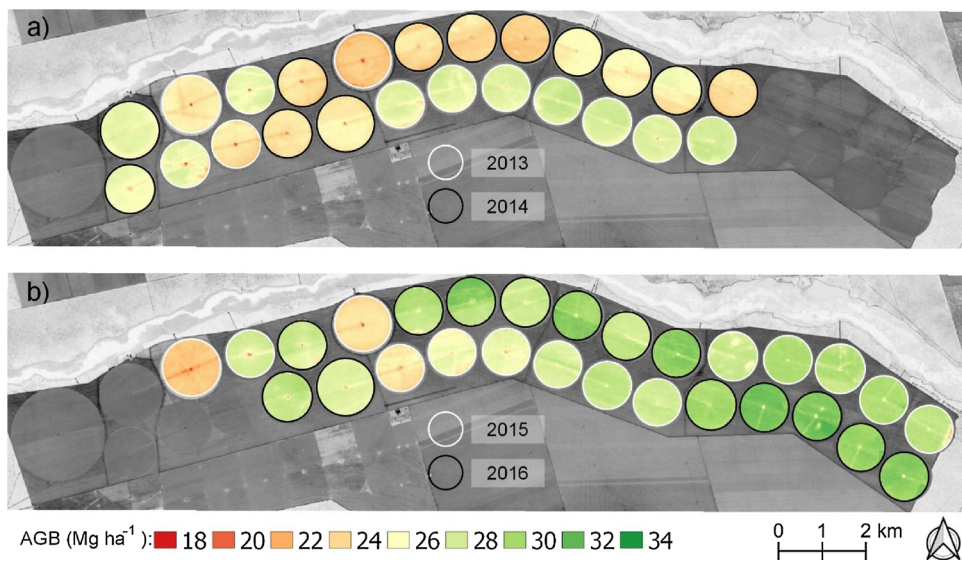


Fig. 10. Map of the accumulated aboveground dry biomass (AGB) of each irrigated corn field in the four consecutive growing seasons (2013–2016). The white circles correspond to the center pivots of 2013 and 2015 and the black circles correspond to center pivots of 2014 and 2016.

Fig. 13a, it is possible to see a good agreement for the Pioneer hybrids, with estimates close to the 1:1 line; the estimated values explained 71% of the variation of the measured data. The RMSE reached 0.536 Mg ha^{-1} , a relatively low value considering the average yield of these hybrids (11.24 Mg ha^{-1} for the 2014, 2015 and 2016 harvests) and a low RRMSE value (4.8%). With MBE = 0.175 Mg ha^{-1} , the overestimates can be considered subtle. In addition, MAE was equal to 0.477 Mg ha^{-1} .

Regarding the Status Viptera 3 hybrid, a reasonable value for r^2 was obtained (0.45). The RMSE (0.705 Mg ha^{-1}) was slightly greater than for Pioneer hybrids, as it also occurred for RRMSE (5.7%) (**Fig. 13b**). The MBE obtained was equal to 0.184 Mg ha^{-1} , which represents an overestimation of the data. The RMSE values obtained for both hybrids were similar to the results found in Holzman and Rivas (2016) and in

Sakamoto et al. (2013). In comparison to the results of Sibley et al. (2014), the RMSE values in the present study are very good since these authors found RMSE values above 2 Mg ha^{-1} for the tested approach and considered it promising.

Fig. 14 shows the absolute difference in the percentages between the estimated and measured values of yield, considering the two groups of hybrids. The highest difference for the Pioneer hybrids was 8.8%, while the smallest values were 0.4 and 0.5% (for the 08A and 10A fields) (**Fig. 14a**). The majority of the values remained between -5 and 5%. The differences in Status Viptera 3 are the same as in **Fig. 12** because HI was maintained equal to 0.45, but here, they were grouped in a single graphic (**Fig. 14b**). Considering the total of 22 center pivot fields, 13 of them (59%) presented values ranging between -5 and 5%, with 90.9% being between -10 and 10%.

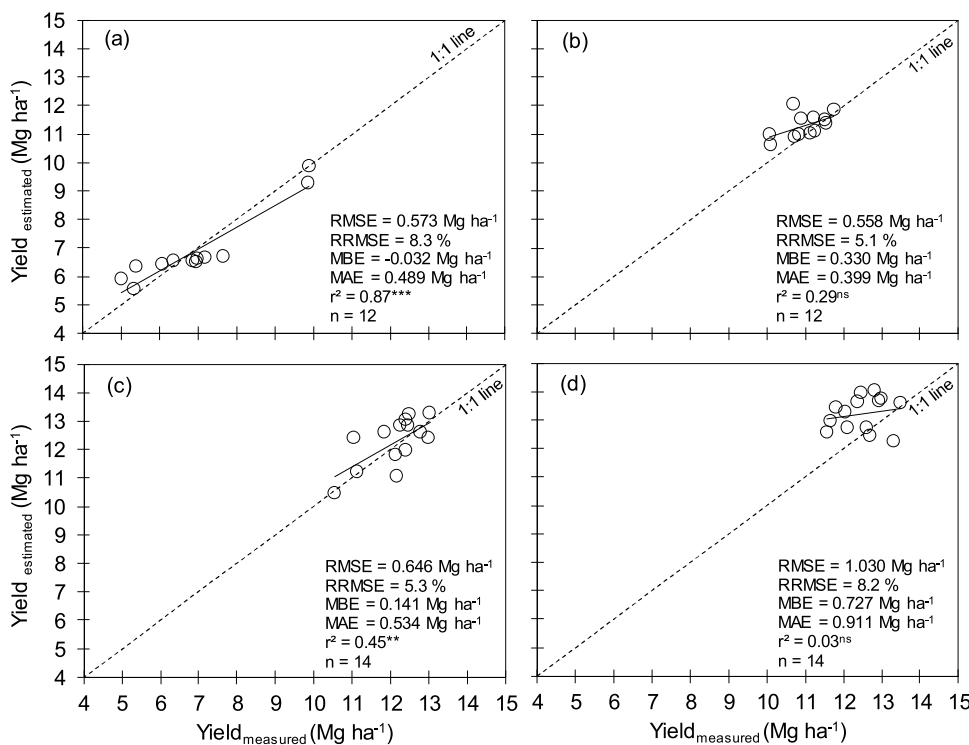


Fig. 11. Measured versus estimated corn grain yields for the growing seasons of 2013 (a), 2014 (b), 2015 (c) and 2016 (d) with the respective statistical parameters, with no separation of hybrids. ^{ns} indicates not significant, * indicates the significance of regression at p-value < 0.05, ** indicates the significance of regression at p-value < 0.01 and *** indicates the significance of regression at p-value < 0.001.

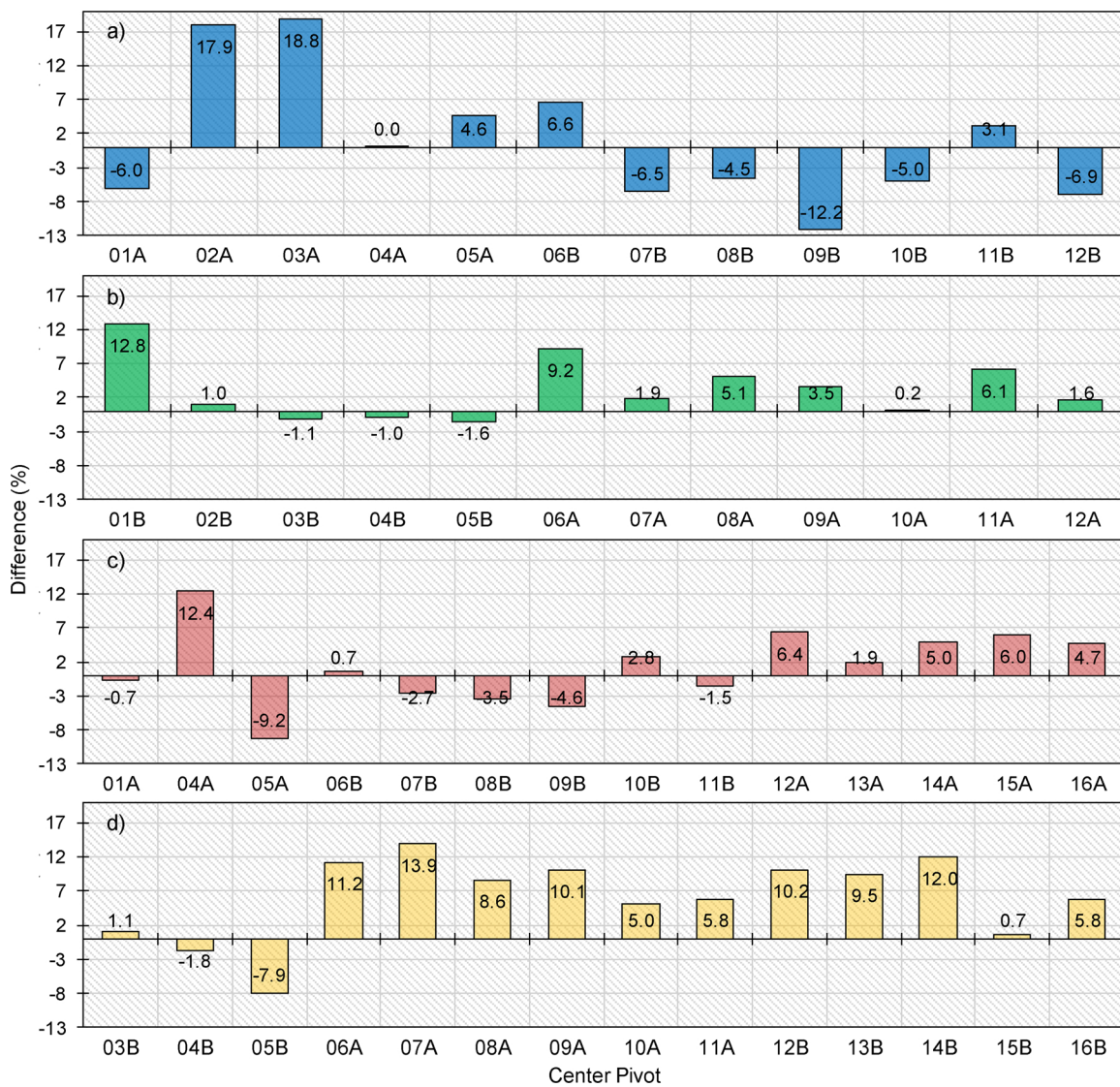


Fig. 12. Percentage difference between the estimated and measured values of yield for each center pivot analyzed in the growing seasons of 2013 (a), 2014 (b), 2015 (c) and 2016 (d).

Overall, the predicted data after the new analysis (*i.e.*, considering two groups of hybrids) can be considered very good, given the complexity of working with field data at the farm level. First, an extensive dataset of 52 center pivot fields was used for the growing seasons, which were not subject to the same controls as an experiment involving small plots, where manual harvesting can be carried out with high

precision. In these 52 fields, harvesting machines may have led to considerable losses. A previous study by Loureiro et al. (2012) demonstrated that losses in corn during mechanized harvesting can reach 8.2%.

In addition, the fields were fully harvested (*i.e.*, including their boundaries), which were excluded from our analysis, to avoid border

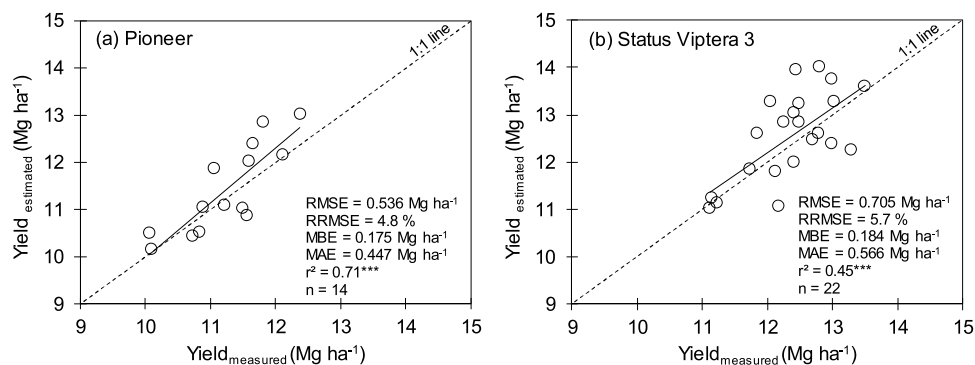


Fig. 13. The measured versus estimated yields of corn grains for the growing seasons of 2014, 2015 and 2016 with the respective statistical parameters, grouped by hybrids. *** indicates significance of regression at p-value < 0.001.

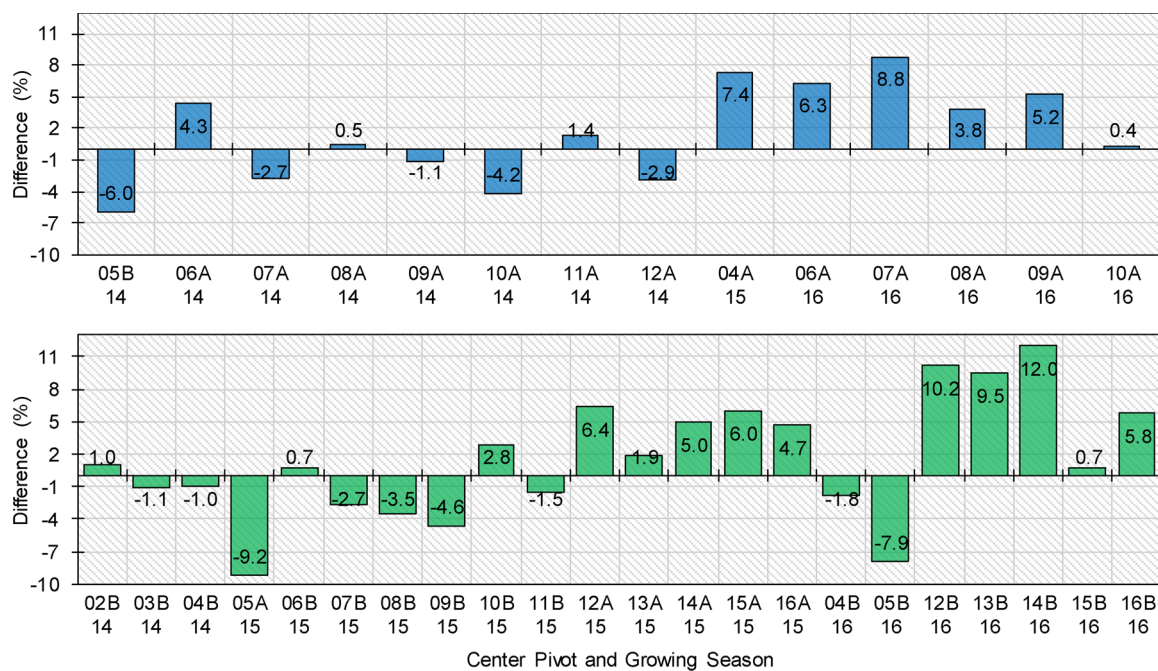


Fig. 14. The percentage difference between estimated and measured values of yield, considering the two groups: (a) Pioneer hybrids and (b) Status Viptera 3, using an HI of 0.43 for Pioneer hybrids, while a value of 0.45 was maintained for Status Viptera 3.

effects. Thus, these facts explain part of the difference in the yield estimates. Although the problems cited above occurred, the present work is considered very useful, especially because of its applicability to the real conditions of field production. According to Sibley et al. (2014), for RS to be useful for analyzing crop yield gaps, methods should be accurate at the field scale without the need for local ground calibration.

3.6. Yield zone map

Within precision agriculture, management zone delineation using RS data is reliable and feasible (Song et al., 2009). The predicted yield maps of the four growing seasons are presented in Fig. 15. These maps were created using two HI for 2013 corn harvest (0.24 and 0.37), 0.43 for the Pioneer hybrids and 0.45 for Status Viptera 3 and other hybrids (see Table 1), as previously discussed. These maps showed a considerable variation in yield among all fields and low variation among individual fields, normally among two or three zones by center pivots (Fig. 15).

It was not possible to clearly observe a pattern of yield class distributed across the field, although the boundaries are commonly regions of low yield. However, after increasing the scale for two fields, more details can be seen. For example, low yield zones were verified in the lower Fig. 15c in all center pivot boundaries. With respect to the upper center pivot highlighted, two patterns are visible: very distinct and individually uniform, which can be a consequence of the sowing of different hybrids or of different water and fertilization management for each slice of the center pivot. Additionally, it is important to highlight that some yield variability is a consequence of natural soil differences (e.g., soil patches). Additionally, there was a notable trend of yield increase over the years, mainly due to technological advancements such as fertilization, irrigation management and weed control.

These yield zone maps can be very useful during harvesting because they can be implemented in the use of the harvesting machine, and thus, the harvest can be carried out by yield zones. Different yields sometimes require different settings of the machines, so one can avoid harvesting the entire area as though yield were uniform and, consequently, the losses can

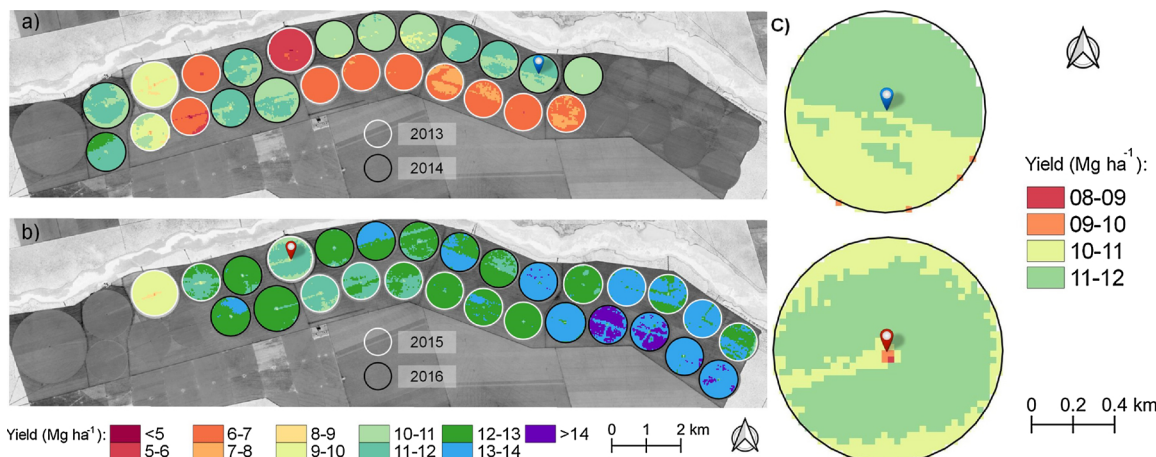


Fig. 15. Predicted yield zone map of each irrigated corn field in the four consecutive growing seasons (a and b) and zoom focus on two fields to highlight the details (c). In Figures a and b, the white circles correspond to center pivots of 2013 and 2015 and the black circles to center pivots of 2014 and 2016.

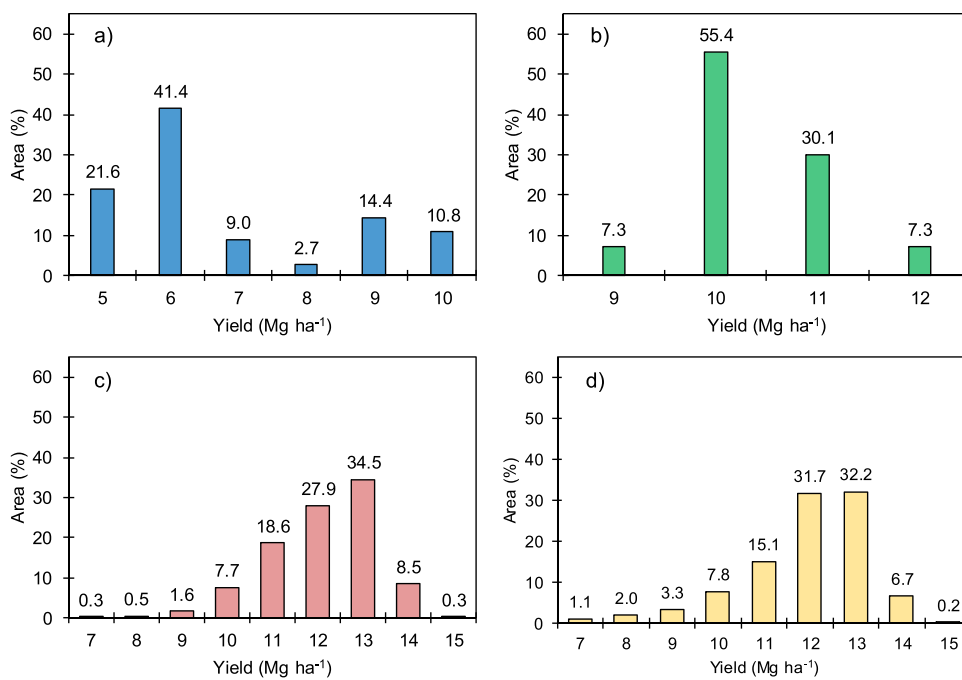


Fig. 16. The percentage area of the center pivots according to corn yield average values for the growing seasons of 2013 (a), 2014 (b), 2015 (c) and 2016 (d).

be decreased during this step. Yield maps are also a valuable archive of field performance and the changes that management might have had on the fields (Franzen, 2018). In addition, yield maps are a reference for the next planting and can help in decisions about soil fertility correction and compaction soil analysis, among other things.

Fig. 16 shows the percentage of area referring to each yield interval, which is important information for decision-making. In 2013 (Fig. 16a), more than 60% of the areas had $5 \leq \text{yields} < 7.0 \text{ Mg ha}^{-1}$. Although these values are compatible with the Brazilian average corn yield (CONAB, 2018), they are very low considering that they are from irrigated plantations, which normally produce more than 10 Mg ha^{-1} . These low values are a consequence of the disease and reinforce that agriculture is a high-risk activity where the producers may have their production reduced by several factors (e.g., disease, pest, drought, excess of rainfall, among others).

With respect to 2014, 2015 and 2016, which were normal production years, the yields were mostly greater than 10 Mg ha^{-1} (Fig. 16b-d). In 2014, only 7.3% produced less than 10 Mg ha^{-1} (Fig. 16b), and in 2015, almost 63% of the area had yields in the range of $12 \text{ to } 13 \text{ Mg ha}^{-1}$ (Fig. 16c). In 2016, there were more yield classes, with variation from 7 to 15 Mg ha^{-1} , but there were similarities to the years 2014 and 2015, with mostly yields of approximately 12 Mg ha^{-1} . The predominance of corn fields with yields of approximately 12 Mg ha^{-1} for these years allowed them to be considered to have high production since the Brazilian average is 5.058 Mg ha^{-1} , considering the 2017/18 harvesting data and the involvement of irrigated and rainfed fields (CONAB, 2018). In addition, the yield zone analysis highlights the potential of using precision agriculture for the enhancement of productivity through managing the low yield locations for greater profitability (Al-Gaadi et al., 2016).

4. Conclusions and remarks

The remote sensing-based model for forecasting corn yield at the farm scale based on the basal crop coefficient that was adjusted to water and cold temperature stress ($K_{cb,adj}$) and the water use efficiency for biomass production (WUE^*_B) parameters were evaluated using surface reflectance images from Landsat 7 and 8 satellites in four growing seasons involving 52 center pivots in corn fields. This study evaluated an extensive dataset of yield combined with the precise knowledge of

the boundaries of the center pivots to perform rigorous testing of the remote sensing estimates of corn yields for a commercial farm that employs a high level of technology in its production processes.

Compared to the original model of Campos et al. (2018a,b), the present work brings the following innovative aspects: (i) calibration to farm level conditions; (b) easy methodology for water stress coefficient determination in comparison with the approach proposed in the FAO-56 manual and (c) the new method for performing the K_{cb} calculation considering the importance of photoassimilate translocation during the reproductive period. The results obtained are useful for analyzing crop yield in corn plantations established in Brazilian farms.

The agreement between the observed and predicted yields was the highest when similar hybrids were grouped, especially for the Pioneer hybrids, with the majority of the differences between predicted yield values and measured yield values remaining between -5 and 5%. However, the prediction could be better if some practices were different. The first change would be a corn harvesting process that would not cause losses (e.g., manual harvesting in small plots). Another practice is the utilization of a specific HI for each hybrid, and considering planting density and crop management, among other factors. It would also be important not to include field boundaries in the harvest because, during the zonal statistical analysis, the vector layer of each center pivot had a 30 m buffer, due to the spatial resolution of Landsat. This would explain part of the difference in the yield estimates.

Finally, the obtained results are promising and show that preharvest corn yield forecasting is operationally feasible because it is easy to acquire free satellite images and to implement the model. Preharvest forecasting based on RS data can help in food security, decision-making and export strategies. Yield zone maps can help farmers in their decision-making by identifying problems in areas with low yields and, therefore, allowing them to adjust their management practices.

Future research should consider some of the sources of error cited above. For instance, the use of individual HI values and decreasing the losses during harvesting should be considered, as well as testing of the model in other regions with different hybrids and management. In summary, our study demonstrated that the Campos et al. (2018a,b) model, with some adjustment for application under Brazilian conditions, is able to successfully estimate most of the yields in irrigated corn fields.

Declaration of Competing Interest

The authors declare no conflict of interest.

Acknowledgments

This study was partially financed by the Coordination of Improvement of Higher Education Personnel - Brazil (CAPES) - Finance Code 001 and by the National Council for Scientific and Technological Development - Brazil (CNPq). We thank to the Daugherty Water for Food Global Institute at the University of Nebraska (UNL), where the first author conducted part of his doctoral research. The authors are also grateful to the company IRRIGER - Irrigation Management and Engineering for making the field data available.

References

- AIBA (Association of Farmers and Irrigators of Bahia), 2017. Agricultural Yearbook of Western Bahia region - Crop 2016/2017. Barreiras, BA, Brazil. <http://aiba.org.br/wp-content/uploads/2018/06/anuario-16-17.pdf> (accessed 25 March 2018).
- Al-Gaadi, K.A., Hassaballa, A.A., Tola, E., Kayad, A.G., Madugundu, R., Alblewi, B., Assiri, F., 2016. Prediction of potato crop yield using precision agriculture techniques. *PLoS One* 11, 1–16. <https://doi.org/10.1371/journal.pone.0162219>.
- Allen, R.G., Pereira, L.S., Raes, D., Smith, M., 1998. *Crop Evapotranspiration: Guidelines for Computing Crop Water Requirements*. FAO Irrigation and Drainage Paper No. 56, FAO, Rome, Italy.
- Allison, J.C.S., Watson, D.J., 1966. The production and distribution of dry matter in maize after flowering. *Ann. Bot.* 30, 365–380.
- Alvares, C.A., Stape, J.L., Sentelhas, P.C., De Moraes Gonçalves, J.L., Sparovek, G., 2013. Köppen's climate classification map for Brazil. *Meteorol. Zeitschrift* 22, 711–728. <https://doi.org/10.1127/0941-2948/2013/0507>.
- Bastiaanssen, W.G.M., Ali, S., 2003. A new crop yield forecasting model based on satellite measurements applied across the Indus Basin. *Pakistan Agric. Ecosyst. Environ.* 94, 321–340. [https://doi.org/10.1016/S0167-8809\(02\)00034-8](https://doi.org/10.1016/S0167-8809(02)00034-8).
- Battude, M., Al Bitar, A., Morin, D., Cros, J., Huc, M., Marais Sicre, C., Le Dantec, V., Demarez, V., 2016. Estimating maize biomass and yield over large areas using high spatial and temporal resolution Sentinel-2 like remote sensing data. *Remote Sens. Environ.* 184, 668–681. <https://doi.org/10.1016/j.rse.2016.07.030>.
- Bausch, W.C., 1993. Soil background effects on reflectance-based crop coefficients for corn. *Remote Sens. Environ.* 46, 213–222. [https://doi.org/10.1016/0034-4257\(93\)90096-G](https://doi.org/10.1016/0034-4257(93)90096-G).
- Bernardo, S., 1989. *Manual De Irrigação*, 5th ed. UFV, Viçosa, MG, Brazil.
- Bocianowski, J., Nowosad, K., Szulc, P., 2019. Soil tillage methods by years interaction for harvest index of maize (*Zea mays L.*) using additive main effects and multiplicative interaction model. *Acta Agric. Scand. Sect. B – Soil Plant Sci.* 69, 75–81. <https://doi.org/10.1080/09064710.2018.1502343>.
- Boote, K.J., Jones, J.W., Pickering, N.B., 1996. Potential uses and limitations of crop models I. Model use Res. Tool. *Agron. J.* 716, 704–716. <https://doi.org/10.2134/agronj1996.00021962008800050005x>.
- Campos, I., González-Gómez, L., Villodre, J., González-Piquer, J., Suyker, A.E., Calera, A., 2018a. Remote sensing-based crop biomass with water or light-driven crop growth models in wheat commercial fields. *F. Crop. Res.* 216, 175–188. <https://doi.org/10.1016/j.fcr.2017.11.025>.
- Campos, I., Neale, C.M.U., Arkebauer, T.J., Suyker, A.E., Gonçalves, I.Z., 2018b. Water productivity and crop yield: a simplified remote sensing driven operational approach. *Agric. For. Meteorol.* 249, 501–511. <https://doi.org/10.1016/j.agrformet.2017.07.018>.
- Campos, I., Neale, C.M.U., Suyker, A.E., Arkebauer, T.J., Gonçalves, I.Z., 2017. Reflectance-based crop coefficients REDUX: for operational evapotranspiration estimates in the age of high producing hybrid varieties. *Agric. Water Manag.* 187, 140–153. <https://doi.org/10.1016/j.agwat.2017.03.022>.
- Caviglia, O.P., Melchiori, R.J.M., Sadras, V.O., 2014. Nitrogen utilization efficiency in maize as affected by hybrid and N rate in late-sown crops. *F. Crop. Res.* 168, 27–37. <https://doi.org/10.1016/j.fcr.2014.08.005>.
- CONAB (Companhia Nacional de Abastecimento), 2018. Acompanhamento Da Safra Brasileira De Grãos, Monitoramento Agrícola - Safra 2017. Brasília, DF, Brazil. (accessed 19 June 2018). <http://www.conab.gov.br>.
- Daughtry, C.S.T., Gallo, K.P., Goward, S.N., Prince, S.D., Kustas, W.P., 1992. Spectral estimates of absorbed radiation and phytomass production in corn and soybean canopies. *Remote Sens. Environ.* 39, 141–152.
- Demétrio, C.S., Fornasier Filho, D., Cazetta, J.O., Cazetta, D.A., 2008. Performance of maize hybrids submitted to different row spacing and population densities. *Pesqui. Agropecu. Bras.* 43, 1691–1697. <https://doi.org/10.1590/S0100-204X20080001200008>.
- Djaman, K., Irmak, S., Rathje, W.R., Martin, D.L., Eisenhauer, D.E., 2013. Maize evapotranspiration, yield production functions, biomass, grain yield, harvest index, and yield response factors under full and limited irrigation. *Trans. ASABE* 56, 373–393. <https://doi.org/10.13031/2013.42676>.
- Doraiswamy, P.C., Moulin, S., Cook, P.W., Stern, A., 2013. Crop yield assessment from remote sensing. *Photogramm. Eng. Remote Sens.* 69, 665–674. <https://doi.org/10.14358/pers.69.6.665>.
- Fancelli, A.L., Dourado Neto, D., 2000. *Produção De Milho*, 2nd ed. Agropecuária, Guaíba, RS, Brazil.
- Ferencz, C., Bognár, P., Lichtenberger, J., Hamar, D., Tarcsai, G., Timár, G., Molnár, G., Pásztor, S., Steinbach, P., Székely, B., Ferencz, O.E., Ferencz-Árkos, I., 2004. Crop yield estimation by satellite remote sensing. *Int. J. Remote Sens.* 25, 4113–4149. <https://doi.org/10.1080/01431160410001698870>.
- Foster, T., Gonçalves, I.Z., Campos, I., Neale, C.M.U., Brozović, N., 2019. Assessing landscape scale heterogeneity in irrigation water use with remote sensing and in situ monitoring. *Environ. Res. Lett.* 14, 024004. <https://doi.org/10.1088/1748-9326/aaf2be>.
- Frampton, W.J., Dash, J., Watmough, G., Milton, E.J., 2013. Evaluating the capabilities of Sentinel-2 for quantitative estimation of biophysical variables in vegetation. *ISPRS J. Photogramm. Remote Sens.* 82, 83–92. <https://doi.org/10.1016/j.isprsjprs.2013.04.007>.
- Franzen, D.W., 2018. Yield Mapping and Use of Yield Map Data. NDSU Extension. Fargo, ND, United States (accessed 07 September 2018). <https://www.sbreb.org/wp-content/uploads/2018/05/Yield-Mapping.pdf>.
- Gitelson, A.A., Viña, A., Arkebauer, T.J., Rundquist, D.C., Keydan, G., Leavitt, B., 2003. Remote estimation of leaf area index and green leaf biomass in maize canopies. *Geophys. Res. Lett.* 30, 51–54. <https://doi.org/10.1029/2002GL016450>.
- Guo, C., Zhang, L., Zhou, X., Zhu, Y., Cao, W., Qiu, X., Cheng, T., Tian, Y., 2017. Integrating remote sensing information with crop model to monitor wheat growth and yield based on simulation zone partitioning. *Precis. Agric.* 19, 1–24. <https://doi.org/10.1007/s11119-017-9498-5>.
- Hanway, J.J., 1966. How a Corn Plant Develops, Special Report. 38. Ames, IA, United States.
- Holzman, M.E., Rivas, R.E., 2016. Early maize yield forecasting from remotely sensed Temperature/Vegetation index measurements. *IEEE J. Sel. Top. Appl. Earth Obs. Remote Sens.* 9, 507–519. <https://doi.org/10.1101/JSTARS.2015.2504262>.
- Huang, J., Gómez-Dans, J.L., Huang, H., Ma, H., Wu, Q., Lewis, P.E., Liang, S., Chen, Z., Xue, J.H., Wu, Y., Zhao, F., Wang, J., Xie, X., 2019. Assimilation of remote sensing into crop growth models: current status and perspectives. *Agric. For. Meteorol.* 276–277, 107609. <https://doi.org/10.1016/j.agrformet.2019.06.008>.
- Huete, A.R., 1988. A soil-adjusted vegetation index (SAVI). *Remote Sens. Environ.* 25, 295–309. [https://doi.org/10.1016/0034-4257\(88\)90106-X](https://doi.org/10.1016/0034-4257(88)90106-X).
- Hütsch, B.W., Schubert, S., 2017. Harvest index of maize (*zea mays L.*): Are there possibilities for improvement? In: Sparks, D.L. (Ed.), Advances in Agronomy. Press, Academic, Cambridge, MA, United States, pp. 37–82. <https://doi.org/10.1016/bs.agron.2017.07.004>.
- Hütsch, B.W., Schubert, S., 2018. Maize harvest index and water use efficiency can be improved by inhibition of gibberellin biosynthesis. *J. Agron. Crop Sci.* 204, 209–218. <https://doi.org/10.1111/jac.12250>.
- INMET (Instituto Nacional de Meteorologia), 2018. Brazilian Climatological Normals 1981 - 2010. Instituto Nacional de Meteorologia, Brasília, DF, Brazil (accessed 01 August 2018). http://www.inmet.gov.br/portal/normais_climatologicas/mobile/index.html#p=1.
- Jin, X., Kumar, L., Li, Z., Feng, H., Xu, X., Yang, G., Wang, J., 2018. A review of data assimilation of remote sensing and crop models. *Eur. J. Agron.* 92, 141–152. <https://doi.org/10.1016/j.eja.2017.11.002>.
- Kasampalis, D., Alexandridis, T., Deva, C., Challinor, A., Moshou, D., Zalidis, G., 2018. Contribution of remote sensing on crop models: a review. *J. Imaging* 4, 52. <https://doi.org/10.3390/jimaging4040052>.
- Kross, A., McNairn, H., Lapen, D., Sunohara, M., Champagne, C., 2015. Assessment of RapidEye vegetation indices for estimation of leaf area index and biomass in corn and soybean crops. *Int. J. Appl. Earth Obs. Geoinf.* 34, 235–248. <https://doi.org/10.1016/j.jag.2014.08.002>.
- Levitán, N., Gross, B., 2018. Utilizing collocated crop growth model simulations to train agronomic satellite retrieval algorithms. *Remote Sens. (Basel)* 10, 1968. <https://doi.org/10.3390/rs10121968>.
- Li, J., Xie, R.Z., Wang, K.R., Ming, B., Guo, Y.Q., Zhang, G.Q., Li, S.K., 2015. Variations in maize dry matter, harvest index, and grain yield with plant density. *Agron. J.* 107, 829–834. <https://doi.org/10.2134/agronj14.0522>.
- Lin, H., Chen, J., Pei, Z., Zhang, S., Hu, X., 2009. Monitoring sugarcane growth using ENVISAT ASAR data. *IEEE Trans. Geosci. Remote Sens.* 47, 2572–2580. <https://doi.org/10.1109/TGRS.2009.2015769>.
- Liú, J., Miller, J.R., Pattey, E., Haboudane, D., Strachan, I.B., Hinther, M., 2004. Monitoring crop biomass accumulation using multi-temporal hyperspectral remote sensing data. *Int. Geosci. Remote Sens. Symp.* 3, 1637–1640. <https://doi.org/10.1109/IGARSS.2004.1370643>.
- Liú, J., Pattey, E., Miller, J.R., McNairn, H., Smith, A., Hu, B., 2010. Estimating crop stresses, aboveground dry biomass and yield of corn using multi-temporal optical data combined with a radiation use efficiency model. *Remote Sens. Environ.* 114, 1167–1177.
- Lizaso, J.I., Batchelor, W.D., Boote, K.J., Westgate, M.E., 2005. Development of a leaf-level canopy assimilation model for CERES-Maize. *Agron. J.* 97, 722–733. <https://doi.org/10.2134/agronj2004.0171>.
- Loureiro, D.R., Fernandes, H.C., Teixeira, M.M., Leite, D.M., Fernandes, L.S., 2012. Quantitative losses in mechanized harvesting corn crop in small footprint and conventional. *Semin. Agrar.* 33, 1351–1358. <https://doi.org/10.5433/1679-0359.2012v33n4p1351>.
- Lukeba, J.L., Vumilia, R.K., Nkongolo, K.C.K., Mwabila, M.L., Tsumbu, M., 2013. Growth and leaf area index simulation in maize (*Zea mays L.*) under small-scale farm conditions in a Sub-Saharan African region. *Am. J. Plant Sci.* 04, 575–583. <https://doi.org/10.4236/ajps.2013.43075>.
- Ma, G., Huang, J., Wu, W., Fan, J., Zou, J., Wu, S., 2013. Assimilation of MODIS-LAI into

- the WOFOST model for forecasting regional winter wheat yield. *Math. Comput. Model.* 58, 634–643. <https://doi.org/10.1016/j.mcm.2011.10.038>.
- Maas, S.J., 2010. Using satellite data to improve model estimates of crop yield. *Agron. J.* 102, 80, 655. <https://doi.org/10.2134/agronj1988.00021962008000040021x>.
- Mantovani, E.C., Bernardo, S., Palaretti, L.F., 2006. Irrigação Princípios E Métodos, 1st ed. Editora UFV, Viçosa, MG, Brazil.
- Mantovani, E.C., Costa, L.C., 1998. Manual Do SISDA 2.0, in: Workshop Internacional Sobre Manejo Integrado Das Culturas E Recursos Hídricos. UFV, Viçosa p. 153.
- Martins, K.V., Dourado-Neto, D., Reichardt, K., Favarin, J.L., Sartori, F.F., Felisberto, G., Mello, S.C., 2017. Maize dry matter production and macronutrient extraction model as a new approach for fertilizer rate estimation. *An. Acad. Bras. Cienc.* 89, 705–716. <https://doi.org/10.1590/0001-3765201720160525>.
- Mokhtari, A., Noory, H., Vazifedoust, M., 2018. Improving crop yield estimation by assimilating LAI and inputting satellite-based surface incoming solar radiation into SWAP model. *Agric. For. Meteorol.* 250–251, 159–170. <https://doi.org/10.1016/j.agrformet.2017.12.250>.
- Monteith, J.L., 1972. Solar radiation and productivity in tropical ecosystems. *J. Appl. Ecol.* 9, 947–966.
- O'Shaughnessy, S.A., Andrade, M.A., Evett, S.R., 2017. Using an integrated crop water stress index for irrigation scheduling of two corn hybrids in a semi-arid region. *Irrig. Sci.* 35, 451–467. <https://doi.org/10.1007/s00271-017-0552-x>.
- Pioneer, D., 2017. Central of Products. (accessed 17 October 2017). <http://www.pioneersementes.com.br/milho/central-de-produtos>.
- Raes, D., Steduto, P., Hsiao, T.C., Fereres, E., 2009. *AquaCrop: Reference Manual. Chapter 2, Users guide*. Food and Agriculture Organization of the United Nations, Rome, Italy.
- Raes, D., Steduto, P., Hsiao, T.C., Fereres, E., 2017. *AquaCrop Version 6.0: Reference Manual. Chapter 3, Calculation procedures*. Food and Agriculture Organization of the United Nations, Rome, Italy.
- Rajcan, I., Tollenaar, M., 1999. Source: sink ratio and leaf senescence in maize:I. Dry matter accumulation and partitioning during grain. *F. Crop. Res.* 60, 255–265. [https://doi.org/10.1016/S0378-4290\(98\)00142-7](https://doi.org/10.1016/S0378-4290(98)00142-7).
- Razzaghi, F., Zhou, Z., Andersen, M.N., Plauborg, F., 2017. Simulation of potato yield in temperate condition by the AquaCrop model. *Agric. Water Manag.* 191, 113–123. <https://doi.org/10.1016/j.agwat.2017.06.008>.
- Sadras, V.O., Cassman, K.G., Grassini, P., Hall, A.J., Bastiaanssen, W.G.M., Laborte, A.G., Milne, A.E., Sileshi, G., Steduto, P., 2018. Yield Gap Analysis of Field Crops: Methods and Case Studies. FAO Water Reports No. 41, Rome, Italy.
- Sakamoto, T., Gitelson, A.A., Arkebauer, T.J., 2013. MODIS-based corn grain yield estimation model incorporating crop phenology information. *Remote Sens. Environ.* 131, 215–231. <https://doi.org/10.1016/j.rse.2012.12.017>.
- Sangoi, L., Lech, V.A., Rampazzo, C., Graciatti, L.C., 2002. Dry matter accumulation of maize hybrids under different source:sink ratios. *Pesqui. Agropecu. Bras.* 37, 259–267. <https://doi.org/10.1590/S0100-204X2002000300005>.
- Sangoi, L., Luiz De Almeida, M., Lech, Adilson, V., Luiz, Graciatti, C., Rampazzo, C., 2001. Performance of contrasting cycle maize hybrids as affected by defoliation and plant population. *Sci. Agric.* 58, 271–276. <https://doi.org/10.1590/S0103-90162001000200009>.
- Santos, H.G., Carvalho-Júnior, W., Dart, R., de, O., Ágio, M.L.D., Sousa, J.S., Pares, J.G., Fontana, A., Martins, A.L.S., Oliveira, A.P.O., 2011. O Novo Mapa De Solos Do Brasil: Legenda Atualizada, 1st ed. Documentos 130. Embrapa Solos, Rio de Janeiro, RJ, Brazil.
- Sibley, A.M., Grassini, P., Thomas, N.E., Cassman, K.G., Lobell, D.B., 2014. Testing remote sensing approaches for assessing yield variability among maize fields. *Agron. J.* 106, 24–32. <https://doi.org/10.2134/agronj2013.0314>.
- Soleymani, A., 2018. Corn (*Zea mays* L.) yield and yield components as affected by light properties in response to plant parameters and N fertilization. *Biocatal. Agric. Biotechnol.* 15, 173–180. <https://doi.org/10.1016/j.bcab.2018.06.011>.
- Song, X., Wang, J., Huang, W., Liu, L., Yan, G., Pu, R., 2009. The delineation of agricultural management zones with high resolution remotely sensed data. *Precis. Agric.* 10, 471–487. <https://doi.org/10.1007/s11119-009-9108-2>.
- Soufizadeh, S., Munaro, E., McLean, G., Massignam, A., van Oosterom, E.J., Chapman, S.C., Messina, C., Cooper, M., Hammer, G.L., 2018. Modelling the nitrogen dynamics of maize crops - Enhancing the APSIM maize model. *Eur. J. Agron.* 100, 118–131. <https://doi.org/10.1016/j.eja.2017.12.007>.
- Steduto, P., Hsiao, T.C., Fereres, E., 2007. On the conservative behavior of biomass water productivity. *Irrig. Sci.* 25, 189–207. <https://doi.org/10.1007/s00271-007-0064-1>.
- Steduto, P., Hsiao, T.C., Fereres, E., Raes, D., 2012. *Crop Yield Response to Water*. FAO Irrigation and Drainage Paper 66. FAO, Rome, Italy.
- Vanuytrecht, E., Raes, D., Steduto, P., Hsiao, T.C., Fereres, E., Heng, L.K., Garcia Vila, M., Mejias Moreno, P., 2014. AquaCrop: FAO's crop water productivity and yield response model. *Environ. Model. Softw.* 62, 351–360. <https://doi.org/10.1016/j.envsoft.2014.08.005>.
- Veloso, A., Mermoz, S., Bouvet, A., Le Toan, T., Planells, M., Dejoux, J.F., Ceschia, E., 2017. Understanding the temporal behavior of crops using Sentinel-1 and Sentinel-2-like data for agricultural applications. *Remote Sens. Environ.* 199, 415–426. <https://doi.org/10.1016/j.rse.2017.07.015>.
- Wang, J., Li, X., Lu, L., Fang, F., 2013. Parameter sensitivity analysis of crop growth models based on the extended Fourier Amplitude Sensitivity Test method. *Environ. Model. Softw.* 48, 171–182. <https://doi.org/10.1016/j.envsoft.2013.06.007>.
- Wang, L., Li, X.G., Guan, Z.-H.H., Jia, B., Turner, N.C., Li, F.-M.M., 2018. The effects of plastic-film mulch on the grain yield and root biomass of maize vary with cultivar in a cold semiarid environment. *F. Crop. Res.* 216, 89–99. <https://doi.org/10.1016/j.fcr.2017.11.010>.
- Xie, Y., Wang, P., Bai, X., Khan, J., Zhang, S., Li, L., Wang, L., 2017. Assimilation of the leaf area index and vegetation temperature condition index for winter wheat yield estimation using Landsat imagery and the CERES-Wheat model. *Agric. For. Meteorol.* 246, 194–206. <https://doi.org/10.1016/j.agrformet.2017.06.015>.
- Yang, H., Grassini, P., Cassman, K.G., Aiken, R.M., Coyne, P.I., 2017. Field Crops Research Improvements to the Hybrid-Maize model for simulating maize yields in harsh rainfed environments. *F. Crop. Res.* 204, 180–190. <https://doi.org/10.1016/j.fcr.2017.01.019>.
- Zhai, L., Xie, R., Li, S., Fan, P., 2017. Relationship between population competitive intensity and yield in maize cultivars. *J. Integr. Agric.* 16, 1312–1321. [https://doi.org/10.1016/S2095-3119\(16\)61541-1](https://doi.org/10.1016/S2095-3119(16)61541-1).